

# High order gradient, curl and divergence conforming spaces, with an application to compatible NURBS-based IsoGeometric Analysis

R.R. Hiemstra<sup>a</sup>, R.H.M. Huijsmans<sup>a</sup>, M.I.Gerritsma<sup>b</sup>

<sup>a</sup>Department of Marine Technology, Mekelweg 2, 2628CD Delft

<sup>b</sup>Department of Aerospace Technology, Kluyverweg 2, 2629HT Delft

---

## Abstract

Conservation laws, in for example, electromagnetism, solid and fluid mechanics, allow an exact discrete representation in terms of line, surface and volume integrals. We develop high order interpolants, from any basis that is a partition of unity, that satisfy these integral relations exactly, at cell level. The resulting gradient, curl and divergence conforming spaces have the property that the conservation laws become completely independent of the basis functions. This means that the conservation laws are exactly satisfied even on curved meshes. As an example, we develop high order gradient, curl and divergence conforming spaces from NURBS - non uniform rational B-splines - and thereby generalize the compatible spaces of B-splines developed in [1]. We give several examples of 2D Stokes flow calculations which result, amongst others, in a point wise divergence free velocity field.

*Keywords:*

Compatible numerical methods, Mixed methods, NURBS, IsoGeometric Analysis

---

*Be careful of the naive view that a physical law is a mathematical relation between previously defined quantities. The situation is, rather, that a certain mathematical structure represents a given physical structure. Burke [2]*

## 1. Introduction

In deriving mathematical models for physical theories, we frequently start with analysis on finite dimensional geometric objects, like a control volume and its bounding surfaces. We assign global, 'measurable', quantities to these different geometric objects and set up balance statements. Take for example the global balance in (1), where the total mass/momentum/energy  $E$  inside a control volume  $V$  is only conserved (no change in time) if the in- and outgoing mass/momentum/energy fluxes  $Q$  over the bounding surfaces  $\partial V$  cancel.

$$\frac{\partial}{\partial t} E(V) = Q(\partial V) \xrightarrow{\lim V \rightarrow P} \frac{\partial}{\partial t} e = \operatorname{div} \mathbf{q}. \quad (1)$$

(discrete or global)                      (differential or local)

This is exactly Gauss divergence theorem, depicted in Figure 1c. Other balance equations in  $\mathbb{R}^3$  involve the fundamental theorem of calculus, relating a global quantity associated with a curve  $L$ , to the values of a quantity at the boundary points  $\partial L$ , and Stokes circulation theorem, which relates the amount of rotation in a surface  $S$  to the amount of circulation around the bounding curve  $\partial S$ .

While the association of physical quantities with geometry is clear in the global sense, it remains obscured when the mathematical model is written in local form, in (1), as a differential equation. The local variables, i.e. the source field  $\mathbf{q}$  and density  $e$ , obtained from a limiting process by shrinking the integration domain  $V$  up to a point  $P$ , although mathematically well defined, seem to have lost their geometric significance.

---

*Email addresses:* R.R.Hiemstra@tudelft.nl (R.R. Hiemstra), R.H.M.Huijsmans@tudelft.nl (R.H.M. Huijsmans), M.I.Gerritsma@tudelft.nl (M.I.Gerritsma)

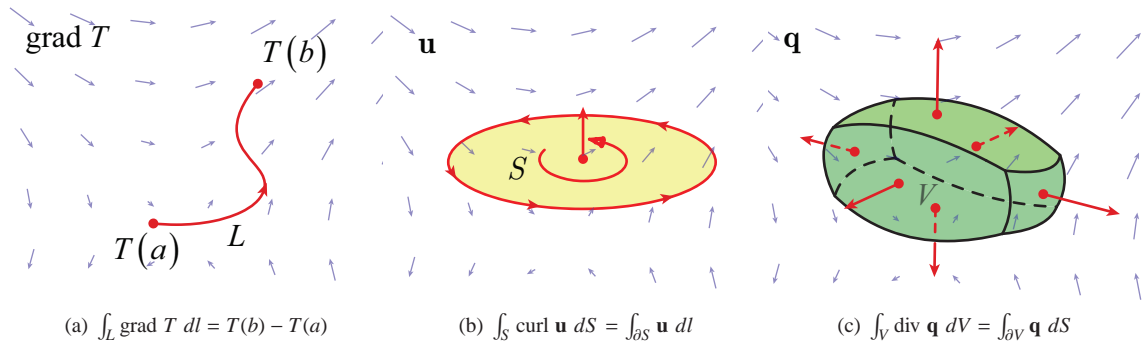


Figure 1: The fundamental theorem of calculus, Stokes circulation theorem and Gauss divergence theorem.

Classical numerical methods, in particular finite difference and nodal finite element methods, take the differential statement as a starting point for discretization. These methods expand their unknowns in terms of nodal interpolations only, and thereby disregard the underlying geometry of the physics. This can lead to instabilities, and perhaps more dangerously, to internal inconsistencies such as the violation of fundamental conservation principles. Where instabilities lead to outright failure of a numerical method, inconsistencies can lead to unphysical solutions that can go unnoticed by the human eye [3]. This becomes more and more pronounced, as the trend is to simulate increasingly larger and complex non-linear phenomena, like multi-phase flows, fluid structure interaction and magnetohydrodynamics.

To capture the behavior of a physical phenomena well, a discretization method should't only approximate the spaces of the infinite dimensional system, but should also follow the structure induced by the relations between them; in particular the structure induced by the fundamental balance equations depicted in Figure 1. By choosing degrees of freedom, not solely associated with nodes, but also with edges, faces and volumes in the mesh, we are able to exactly satisfy these relations in the discrete setting.

We follow the pioneering work of Tonti [4, 5], Mattiussi [6], Bossavit [7, 8] and the recent advances in *Discrete Exterior Calculus* [9, 10], *Finite Element Exterior Calculus* [11, 12], *Compatible* [1, 13, 14, 15, 16] and *Mimetic Methods* [17, 18, 19, 20, 21, 22, 23, 24]. These methods, do not focus on one particular physical problem, but identify and discretize the underlying structure that constitutes a wide variety of physical field theories. They are said to be 'compatible' with the geometric structure of the underlying physics, i.e. they 'mimic' important properties of the physical system. This leads, amongst others, to naturally stable and consistent numerical schemes that have discrete conservation properties by construction and are applicable to a wide variety of physical theories. Furthermore, they offer insight into the properties of existing numerical schemes.

We develop arbitrary order interpolants, starting from any basis that is a partition of unity, which satisfy the fundamental integral theorems exactly. The gradient, curl and divergence conforming spaces have the property that the conservation laws become completely independent of the basis functions. This means that the conservation laws are exactly satisfied at the coarsest level of discretization and on arbitrarily curved meshes. It is remarkable that inf-sup stability is automatically guaranteed when this physical structure is encoded in the discretization [22, 23].

As an example we apply our approach to NURBS (non-uniform rational B-splines) and thereby generalize the compatible spaces of B-splines introduced in [1]. NURBS, the standard in Computer Aided Design (CAD), have only recently become popular in the finite element community due to the very successful IsoGeometric Analysis (IGA) paradigm [25]. IGA employs CAD technologies, such as B-splines and NURBS, directly within the finite element spaces, and thereby integrates computer aided design with finite element analysis (FEA). IsoGeometric Analysis not only bridges the gap between CAD and FEA, it also provides exact geometry representation at the coarsest level of discretization [25]; possesses increased robustness and accuracy [26]; and refining strategies become practically applicable [25]. Development is ongoing and IsoGeometric Analysis has over the years reached a certain level of maturity. For an overview we refer the reader to [27].

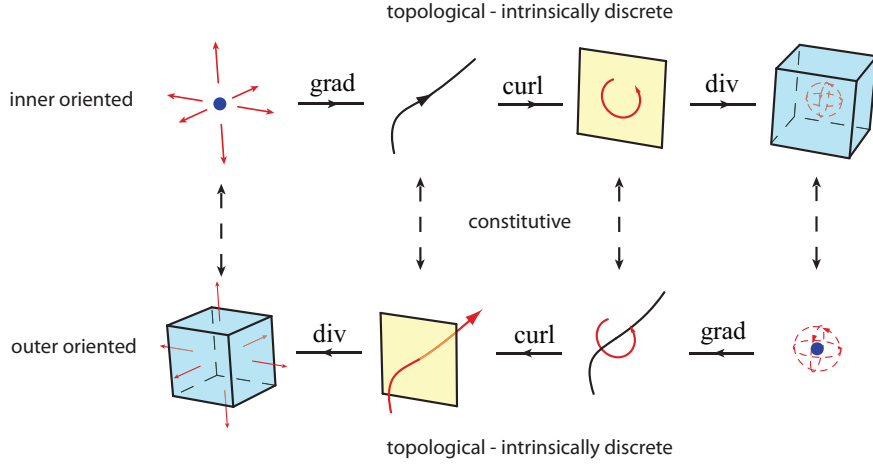


Figure 2: Physical quantities in  $\mathbb{R}^3$  can be associated with either inner or outer oriented points, curves, surfaces and volumes. They are horizontally connected by means of the balance equations, i.e. fundamental theorem of calculus, Stokes circulation theorem and Gauss divergence theorem, which are metric free. The metric and material dependent relations, i.e. the constitutive equations represent the relation between physical quantities associated with dual geometric objects.

### 1.1. Geometric structure of partial differential equations (PDE's)

Geometry induces physics with a clear geometric structure. Consider Figure 2. Physical quantities are naturally related to geometric objects such as points, curves, surfaces and volumes. Furthermore, we can consider two separate types of orientation with respect to the geometric object: inner and outer orientation. Temperature, for example, is measured in a point; strain of a fiber along a curve; magnetic flux through a surface; mass flowing out of a volume; and an amount of rotation in a surface. Note there is room for interpretation since an amount of rotation could similarly be associated with a vortex filament.

Physical quantities are horizontally connected by the fundamental theorem of calculus, Stokes circulation theorem and Gauss divergence theorem (Figure 1). These balance equations can exactly be described in terms of discrete physical quantities, that could have been obtained from some measurement process, and besides are independent of the shape of the geometry; i.e. they are intrinsically discrete and topological in nature.

The metric, notions of length, area, volume, angle, along with material properties of the medium, are described by the constitutive equations, which require a differential formulation. These represent the relations between physical quantities associated with dual geometric objects. Consider for example Hooke's law which relates the strain of a fiber along an inner oriented curve, with the stress through an outer oriented surface. Another example is the proportional relationship between point-wise defined temperature and kinetic energy contained in a volume for a perfect gas.

The schematic in Figure 2 can serve as a template to design compatible numerical methods for partial differential equations (PDE's). By reformulating a PDE in terms of a set of first order equations one can distinguish between the topological nature of the balance laws and the metric nature of the constitutive equations. This idea is by no means new. In fact, Figure 2 is known as a Tonti diagram, after Enzo Tonti. For more details, we refer the reader to the work of Tonti [4] and Mattiussi [6].

We consider Stokes flow in a domain  $\Omega$ , filled with an incompressible fluid with constant viscosity  $\nu$ . Under these assumptions, Stokes flow can be described by the following equations,

$$\nu \Delta \mathbf{u} - \text{grad } p = \mathbf{f} \quad \text{and} \quad \text{div } \mathbf{u} = 0, \quad (2)$$

where  $\mathbf{u}$  is the velocity,  $p$  the pressure and  $\mathbf{f}$  the right hand side forcing. Using the operator splitting,  $-\Delta \mathbf{u} = \text{curl curl } \mathbf{u} + \text{grad div } \mathbf{u}$ , and using the incompressibility constraint,  $\text{div } \mathbf{u} = 0$ , we can decouple Stokes flow into the following first order equations,

$$\text{curl } \mathbf{u} = \boldsymbol{\omega}, \quad \text{curl } \boldsymbol{\omega} + \text{grad } p = -\mathbf{f}, \quad \text{div } \mathbf{u} = 0, \quad (3)$$

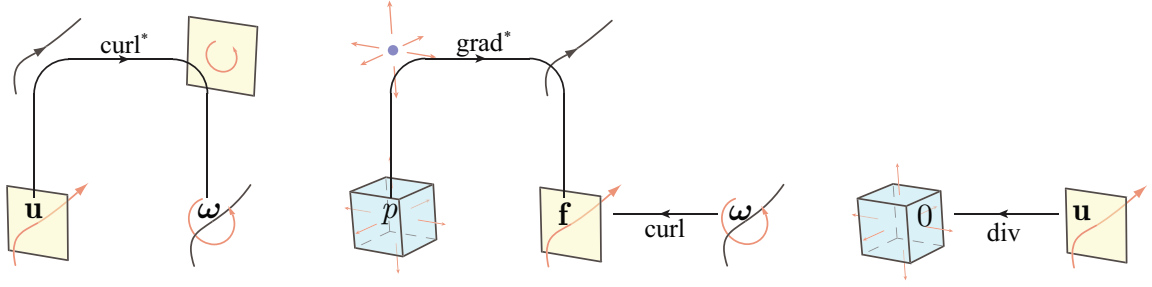


Figure 3: Tonti diagram illustrating mixed formulation for Stokes flow with outer oriented variables. Velocity  $\mathbf{u}$  is associated with outer oriented surfaces, pressure  $p$  is defined in outer oriented volumes and the vorticity  $\omega$  is related to outer oriented lines.

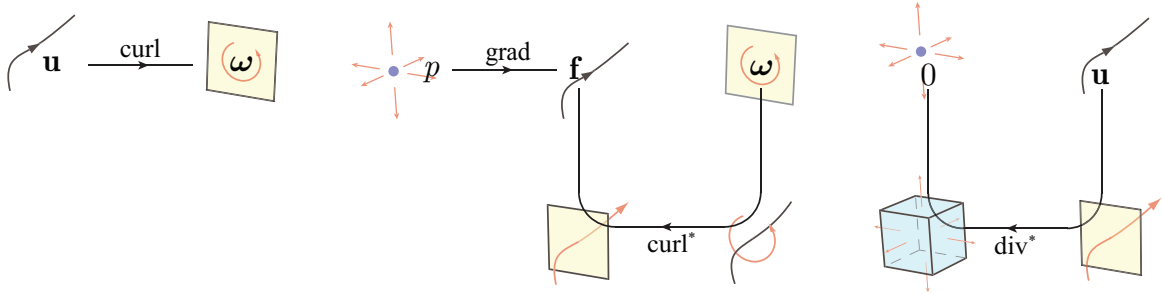


Figure 4: Tonti diagram illustrating mixed formulation for Stokes flow with inner oriented variables. Velocity  $\mathbf{u}$  is associated with inner oriented lines, pressure  $p$  is associated with inner oriented points and the vorticity  $\omega$  is related to inner oriented surfaces.

where  $\omega$  is the vorticity. Observe that Stokes circulation theorem (Figure 1b) means that  $\mathbf{u}$  in  $\text{curl } \mathbf{u}$  is associated with inner oriented curves, while Gauss divergence theorem (Figure 1c) implies that  $\mathbf{u}$  in  $\text{div } \mathbf{u}$  is associated with outer oriented surfaces. The variable  $\mathbf{u}$  thus has a different geometric interpretation depending on the type of balance law and needs to be treated accordingly.

It is possible to discretize variables on staggered grids of opposite orientation, as in many finite volume methods, and make an explicit relation between quantities associated with dual geometric objects. We will however follow a more finite element type of method and circumvent the use of a dual (staggered) grid by using integration by parts. While  $\text{grad}$ ,  $\text{curl}$  and  $\text{div}$  are the differential operators that naturally occur in the fundamental theorem of calculus, Stokes circulation theorem, and Gauss divergence theorem, we can define  $\text{grad}^*$ ,  $\text{curl}^*$  and  $\text{div}^*$  as their formal Hilbert adjoint up to a possible boundary term [21],

$$(\alpha, -\text{grad}^* \beta) = (\text{div } \alpha, \beta), \quad (\gamma, \text{curl}^* \delta) = (\text{curl } \gamma, \delta), \quad (\epsilon, -\text{div}^* \zeta) = (\text{grad } \epsilon, \zeta) \quad (4)$$

While the  $\text{grad}$ ,  $\text{curl}$  and  $\text{div}$  operators are purely topological (metric free) and allow an exact discrete representation (Section 3), the  $\text{grad}^*$ ,  $\text{curl}^*$  and  $\text{div}^*$  are metric dependent and can only be approximated in the discrete setting.

We can use these operators in a mixed Galerkin setting, where the resulting mixed formulation depends solely on physical considerations. Take for example the mixed formulation of the Stokes problem depicted in Figure 3, where the variables are associated with outer oriented geometric elements. In this case we apply the topological equation  $\text{div } \mathbf{u} = 0$  for conservation of mass, which will eventually give a point-wise divergence free velocity field in the discrete setting. Furthermore, inflow boundary conditions can be enforced strongly, while tangential velocity is prescribed in a weak sense.

We could also choose to associate all variables with inner oriented geometric elements. This mixed formulation is shown in Figure 4. In this case the equation  $\text{curl } \mathbf{u} = \omega$  is topological and allows an exact discrete representation. Furthermore, tangential velocity can be enforced strongly, while normal velocity is prescribed in a weak sense.

The paper is structured as follows. In Section 2 we introduce differential forms as the natural mathematical objects representing physical fields. Differential forms allow a continuous description of physics that maintains its

geometric content and allows us to separate the topological from the metric dependent structure. Topological structure is intrinsically discrete, and can exactly be encoded in terms of discrete objects known as chains (discrete geometric objects) and cochains (discrete quantities), see Section 3. Metric structure, on the other hand, requires a continuous description. In Section 4, we derive a new procedure to develop high order cochain interpolants, from any basis that is a partition of unity, that by construction satisfy the balance laws. As an example, we develop high order gradient, curl and divergence conforming basis functions from NURBS and apply these newly developed spaces in a mixed Galerkin setting, Section 5, to Stokes flow and perform some numerical calculations to assess the numerical approach (section 6); finally, conclusions are drawn in section 7.

## 2. Differential modeling

The mathematical description of physical phenomena such as electromagnetism, solid and fluid mechanics, relies heavily on the use of line, surface and volume integrals. The differential objects that appear as their integrands are called differential forms (see Example 2.1), and are studied in the mathematical field of differential geometry [2, 28, 29].

A description of physics in terms of differential forms offers significant benefits. Most notable, differential forms maintain a clear relation with the underlying geometry and therefore allow a separation of the metric dependent content, of a physical theory, from its topological (metric-free) part. This relation with geometry also makes it possible to transfer operations on the geometry to operations on the variables associated with that geometry. Furthermore, representation of variables in terms of differential forms offers a generalized concept of derivative, and thereby reduces the fundamental theorem of calculus, Stokes circulation theorem and Gauss divergence theorem to one equation, known as the generalized Stokes theorem. Most material presented in this section can be found in the references cited above.

### 2.1. Differential forms

Consider a sufficiently smooth  $n$ -dimensional domain  $\Omega$  with boundary  $\partial\Omega$  and local coordinates  $\mathbf{x} = (x^1, x^2, \dots, x^n)$ . A  $k$ -form  $a^k$  is a mathematical expression of the following form,

$$a^k = \sum_I a_I(\mathbf{x}) dx^I \quad \text{with} \quad dx^I = dx^{i_1} \wedge dx^{i_2} \wedge \dots \wedge dx^{i_k}, \quad (5)$$

where the indices satisfy,  $1 \leq i_1 \leq i_2 \leq \dots \leq i_k \leq n$ , the  $a_I(\mathbf{x})$  are smooth functions that denote the spatial distribution of some physical quantity, and the basis elements  $dx^I$  refer to the associated geometry. The collection of all  $k$ -forms is a vector space  $\Lambda^k(\Omega)$  of dimension equal to the binomial coefficient  $\binom{n}{k}$ . Some examples of differential forms in  $\mathbb{R}^3$  are depicted below.

**Example 2.1 (Differential forms in  $\mathbb{R}^3$ ).** *Temperature,  $T^0$ , is a 0-form, a scalar function that assigns to every point  $\mathbf{x}$  in domain  $\Omega$  a real valued temperature; force,  $F^1$ , is a 1-form, since it can naturally be integrated along a curve to obtain work; flux density,  $Q^2$ , is a 2-form and can be integrated over a surface to obtain the global flux; mass density  $\rho^3$ , is a 3-form, since it is readily integrated over a volume to yield mass.*

<b>0-form</b>	<i>Temperature:</i>	$T^0 = T(\mathbf{x}),$
<b>1-form</b>	<i>Force density</i>	$F^1 = f_1(\mathbf{x})dx^1 + f_2(\mathbf{x})dx^2 + f_3(\mathbf{x})dx^3,$
<b>2-form</b>	<i>Flux density</i>	$Q^2 = q_1(\mathbf{x})dx^2 \wedge dx^3 + q_2(\mathbf{x})dx^3 \wedge dx^1 + q_3(\mathbf{x})dx^1 \wedge dx^2,$
<b>3-form</b>	<i>Mass density</i>	$\rho^3 = \rho(\mathbf{x})dx^1 \wedge dx^2 \wedge dx^3.$

The  $\wedge$ , is called the wedge product, which is a map,  $\wedge : \Lambda^k(\Omega) \times \Lambda^l(\Omega) \mapsto \Lambda^{k+l}(\Omega)$ ,  $k+l \leq n$ . The wedge product is skew symmetric,  $a^k \wedge b^l = (-1)^{k+l} b^l \wedge a^k$ . So,  $dx^i \wedge dx^j = -dx^j \wedge dx^i$ , which implies that the orientation changes under a permutation of the elements and linear independence, since  $dx^i \wedge dx^i = -dx^i \wedge dx^i = 0$ .

$k$ -forms are the natural integrands over  $k$ -dimensional geometric objects,

$$\langle a^k, \Omega_k \rangle := \int_{\Omega_k} a^k \in \mathbb{R} \quad (6)$$

Here  $\langle \cdot, \cdot \rangle$  denotes duality pairing between the  $k$ -form and a  $k$ -dimensional geometric object. This duality, between geometry and physics has important consequences. It induces physics with a clear geometric structure. This allows us to separate the metric and material dependent content in a physical theory from the topological, metric independent part. Furthermore, it makes it possible to transfer operations on the geometry to operations on the variables associated with that geometry.

## 2.2. Topological structure

Integration itself is a metric free operation. If  $\Phi : \Omega' \mapsto \Omega$ , is a smooth map from an  $n$ -dimensional reference domain  $\Omega' = [0, 1]^n$  to the  $n$ -dimensional physical domain  $\Omega$ , the pullback,  $\Phi^* : \Lambda^k(\Omega) \mapsto \Lambda^k(\Omega')$ , maps  $k$ -forms on  $\Omega$  to  $k$ -forms on  $\Omega'$ . This means we can perform the integration of a  $k$ -form in the reference domain  $\Omega'$ ,

$$\int_{\Phi(\Omega'_k)} a^k = \int_{\Omega'_k} \Phi^* a^k \iff \langle a^k, \Phi(\Omega'_k) \rangle = \langle \Phi^* a^k, \Omega'_k \rangle. \quad (7)$$

This means that the pullback  $\Phi^*$  is the formal adjoint of the map  $\Phi$  in the duality pairing defined in (6). Important properties of the pull back are linearity and commutation with the wedge product,  $\Phi^*(a^k \wedge b^l) = (\Phi^* a^k) \wedge (\Phi^* b^l)$ .

Topological structure is induced by balance laws, which relate a quantity associated with a geometric object to another quantity which is associated with its boundary. In the theory of differential forms, this balance is represented by the generalized Stokes theorem, the mother of all equations,

$$\int_{\Omega_k} d\omega^{k-1} = \int_{\partial\Omega_k} \omega^{k-1} \iff \langle d\omega^{k-1}, \Omega_k \rangle = \langle \omega^{k-1}, \partial\Omega_k \rangle. \quad (8)$$

Again we can observe the duality between geometry and physics: the boundary operator,  $\partial$ , is the adjoint of the exterior derivative  $d$ . While the boundary operator is a map  $\partial : \Omega_k \mapsto \Omega_{k-1}$ , the exterior derivative is a map,  $d : \Lambda^{k-1}(\Omega) \mapsto \Lambda^k(\Omega)$ .

The exterior derivative  $d$  is a coordinate independent generalization of the well known vector calculus identities, the gradient, curl and divergence operators in  $\mathbb{R}^3$ . The Stokes theorem (8) thus generalizes the fundamental theorem of calculus ( $k = 1$ ), Stokes circulation theorem ( $k = 2$ ) and Gauss divergence theorem ( $k = 3$ ), depicted in Figure 1. Furthermore, the exterior derivative is no more difficult to compute in a curved coordinate system than it is in a Cartesian frame. One simply takes the differential of the components and follows the properties of the wedge product.

**Example 2.2 (Action of the exterior derivative in  $\mathbb{R}^3$ ).** Consider local coordinates  $(x^1, x^2, x^3)$ . The action of the exterior derivative on the 0-form  $T^0$ , 1-form  $F^1$  and 2-form  $Q^2$  from Example 2.1, is given by

$$\begin{aligned} dT^0 &= \frac{\partial T}{\partial x^1} dx^1 + \frac{\partial T}{\partial x^2} dx^2 + \frac{\partial T}{\partial x^3} dx^3 \\ dF^1 &= \left( \frac{\partial f_3}{\partial x^2} - \frac{\partial f_2}{\partial x^3} \right) dx^2 \wedge dx^3 + \left( \frac{\partial f_1}{\partial x^3} - \frac{\partial f_3}{\partial x^1} \right) dx^3 \wedge dx^1 + \left( \frac{\partial f_2}{\partial x^1} - \frac{\partial f_1}{\partial x^2} \right) dx^1 \wedge dx^2 \\ dQ^2 &= \left( \frac{\partial q_1}{\partial x^1} + \frac{\partial q_2}{\partial x^2} + \frac{\partial q_3}{\partial x^3} \right) dx^1 \wedge dx^2 \wedge dx^3. \end{aligned}$$

Observe that the components are given by those of the familiar grad, curl and div operators, respectively.

The exterior derivative has a number of important properties: it is a linear operator (9); satisfies a Leibniz rule for differentiation (10); its metric free nature is reflected by commutation with the pull back (11); and is exact (12);

$$d(a^k + b^k) = da^k + db^k \quad (9)$$

$$d(a^k \wedge b^l) = da^k \wedge b^l - (-1)^k a^k \wedge db^l \quad (10)$$

$$d\Phi^* = \Phi^* d \quad (11)$$

$$d \circ d = 0 \quad (12)$$

This last property is analogous to the vector calculus identities,  $\text{curl grad} = 0$  and  $\text{div curl} = 0$ .

The  $n + 1$ -spaces of differential forms in an  $n$ -dimensional domain  $\Omega$ , satisfy the following sequence, known as the *de Rahm* complex,

$$\mathbb{R} \longrightarrow \Lambda^0(\Omega) \xrightarrow{d} \Lambda^1(\Omega) \xrightarrow{d} \dots \xrightarrow{d} \Lambda^n(\Omega) \xrightarrow{d} 0. \quad (13)$$

which is exact on contractible domains. The main focus of this paper, see Section 4, is to construct discrete spaces of differential forms, that follow the same structure, such that conservation and balance laws can be strongly enforced.

### 2.3. Metric structure

Constitutive equations depend on the local metric, notions of length, angle, area, volume etc., and material properties of the medium under consideration. In order to measure the local metric we require a point wise inner product of  $k$ -forms,  $(\cdot, \cdot) : \Lambda^k(\Omega) \times \Lambda^k(\Omega) \mapsto \mathbb{R}$ . In particular, a Riemannian metric gives rise to the Hilbert space  $L^2$  inner product on  $\Lambda^k(\Omega)$ ,

$$(\alpha^k, \beta^k)_\Omega := \int_\Omega (\alpha^k, \beta^k) d\Omega = \int_\Omega \alpha^k \wedge \star \beta^k. \quad (14)$$

Here  $\star$  denotes the Hodge star operator, which is a map  $\star : \Lambda^k(\Omega) \mapsto \Lambda^{n-k}(\Omega)$ .

**Example 2.3 (Action of the Hodge star in  $\mathbb{R}^3$ ).** In  $\mathbb{R}^3$  with orthonormal coordinates  $\mathbf{y} = (y^1, y^2, y^3)$  we have

$$\star 1 = dy^1 \wedge dy^2 \wedge dy^3, \quad \star dy^1 \wedge dy^2 \wedge dy^3 = 1$$

$$\star dy^1 = dy^2 \wedge dy^3, \quad \star dy^2 = dy^3 \wedge dy^1, \quad \star dy^3 = dy^1 \wedge dy^2.$$

The Hodge not only maps  $k$ -forms into  $(n - k)$ -forms, but also changes its type of orientation from inner to outer and vice versa. We can therefore apply it to connect two copies of an exact sequence into the following structure,

$$\begin{array}{ccccccccc} \mathbb{R} & \longrightarrow & \Lambda^0(\Omega) & \xrightarrow{d} & \Lambda^1(\Omega) & \xrightarrow{d} & \Lambda^2(\Omega) & \xrightarrow{d} & \Lambda^3(\Omega) & \longrightarrow & 0 \\ & & \uparrow \star & & \uparrow \star & & \uparrow \star & & \uparrow \star & & \\ & & \Lambda^3(\Omega) & \xleftarrow{d} & \Lambda^2(\Omega) & \xleftarrow{d} & \Lambda^1(\Omega) & \xleftarrow{d} & \Lambda^0(\Omega) & \xleftarrow{d} & \mathbb{R} \end{array} \quad (15)$$

Note that this is exactly the structure given in Figure 2! While the exterior derivative  $d$  models the topological structure of the balance laws, the Hodge  $\star$  models the metric structure of the constitutive equations.

Using Leibniz's rule for differentiation (10), and noting that a double application of the Hodge star changes nothing up to a possible minus sign,  $\star \star = (-1)^{k(n-k)}$ , we can derive an adjoint operator for the exterior derivative,

$$\begin{aligned} d(\alpha^{k-1} \wedge \star \beta^k) &= d\alpha^{k-1} \wedge \star \beta^k - (-1)^k \alpha^{k-1} \wedge d\star \beta^k \\ &= d\alpha^{k-1} \wedge \star \beta^k - (-1)^{n(k+1)+1} \alpha^{k-1} \wedge \star (\star d\star) \beta^k, \end{aligned}$$

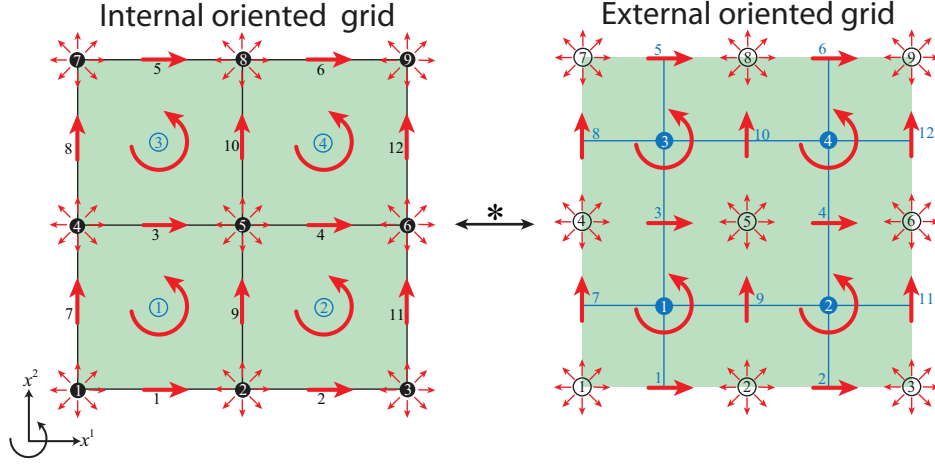


Figure 5: The discrete Hodge invokes a connection between variables associated with dual geometric objects.

where  $d^* = (-1)^{n(k+1)+1} \star d \star$  is the codifferential. Using the inner product property of the Hodge (14) and using integration by parts, we find that the codifferential is the Hilbert adjoint of the exterior derivative with an additional boundary term,

$$(d\alpha^{k-1}, \beta^k)_\Omega - (\alpha^{k-1}, d^*\beta^k)_\Omega = \int_{\partial\Omega} \alpha^{k-1} \wedge \star\beta^k. \quad (16)$$

The coderivative  $d^*$  is thus a generalization of the  $\text{grad}^*$ ,  $\text{curl}^*$  and  $\text{div}^*$  introduced in (4). Equation (16) will prove to be very important in the mixed Galerkin setting explained in Section 5. The exterior derivative and codifferential can be combined to construct the Laplacian  $\Delta$ . The Hodge Laplacian is a map,  $\Delta : \Lambda^k(\Omega) \mapsto \Lambda^k(\Omega)$ ,

$$\Delta = dd^* + d^*d. \quad (17)$$

### 3. Discrete modeling

Classical numerical methods, in particular finite difference and nodal finite element methods, expand their unknowns in terms of nodal interpolations and run into trouble when it comes to conservation. Conservation, by definition (Generalized Stokes theorem (8)) is a relation between a global 'measurable' quantity associated with a geometric object and another global 'measurable' quantity associated with its boundary. By choosing degrees of freedom associated with nodes, as well as edges, faces and volumes in the mesh, we are able to exactly satisfy these relations in the discrete case.

The constitutive equations describe a relation between physical quantities associated with dual geometric objects. In discrete space, this is modeled by a discrete Hodge  $*$  operator which invokes a relation between staggered grids of opposite orientation, see Figure 5. Staggered finite volume methods explicitly build such a dual (staggered) grid and thus explicitly construct a discrete Hodge to connect variables on both grids. In this paper we use a Galerkin finite element type of approach and circumvent the use of a dual grid by applying integration by parts, using (16).

In this section we introduce geometry in terms of algebraic topology [30, 31]. Topology describes the relations between oriented geometric objects (chains) and what 'lives' on those objects (cochains), however, without the notion of distance or measure. Algebraic topology thus allows us to encode the purely discrete and topological content of the physics into the discrete model, without any approximation.

Algebraic topology can in many ways be regarded as the discrete analogous of differential geometry. The duality pairing between chains and cochains is analogue to that of integration of differential forms. By defining a formal adjoint of the boundary of a chain, we obtain a discrete derivative acting on cochains, known as the coboundary operator. This discrete derivative is constructed such that it exactly satisfies Stokes theorem in terms of chains and



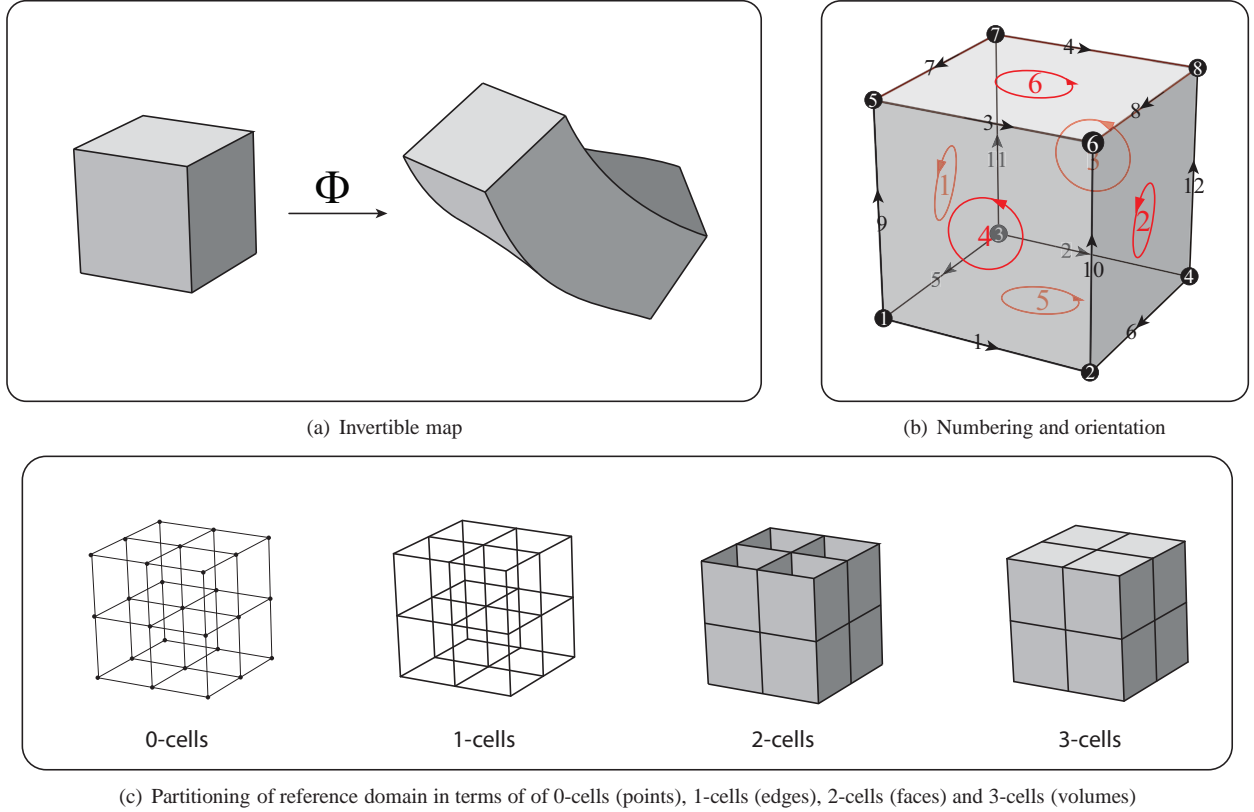


Figure 6: (a) The curved domain  $\Phi(\Omega') = \Omega$  has the same topology as the reference domain  $\Omega'$ . (c) Once the reference domain  $\Omega'$  is partitioned into 0-cells (points), 1-cells (edges), 2-cells (faces) and 3-cells (volumes), every cell can be given an arbitrary numbering and orientation (b).

cochains. Because all objects and operators that will be introduced in this section are topological and thus completely metric-free, they have the same form and value on topologically equivalent grids. The discretization of these relations is equivalent on a nice uniform Cartesian mesh as it is on a highly curved grid. Furthermore, they do not change on moving meshes as long as the topology stays the same.

### 3.1. Cell complexes, chains and the boundary operator

The pairing between physical quantities and oriented geometric objects, such as points, edges, faces and volumes, leads to a straightforward discretization of the  $n$ -dimensional computational domain  $\Omega$ . The topological description of  $\Omega$  is given by a so called cell complex  $D$ , a formalized concept of the discretization of space, which is a partitioning in terms of  $k$ -dimensional sub-domains ( $k = 0, \dots, n$ ) called  $k$ -cells, which we denote by  $\sigma_{(k),i}$ .

Figure 6 depicts a cell complex in  $\mathbb{R}^3$ , where we can distinguish between 0-cells (points), 1-cells (edges), 2-cells (faces) and 3-cells (volumes). For the present work it is most convenient to think of a cell complex as a union of  $k$ -cubes. An alternative would be to partition the cell complex in  $k$ -simplices as is done in e.g. [9, 10, 11, 12]. From the topological viewpoint, both descriptions are equivalent [32].

Once all  $k$ -cells in the cell complex  $D$  have been numbered and given an orientation (see Figure 6b), they can be collected to form a  $k$ -chain,  $c_{(k)} \in C_{(k)}(D)$ ,

$$c_{(k)} = \left\{ c^j \cdot \sigma_{(k),j} \right\}_{j=0}^s \quad \text{with } c^j \in \{-1, 0, 1\}. \quad (18)$$

In the representation of a chain we use superscript for the coefficients  $c^j$  and subscript for the basis  $k$ -cells  $\sigma_{(k),j}$ . Chains can be used as a discrete representation of the geometry. In the description of geometry, however, we will only

be concerned with chains with coefficients,  $c^j$  of  $\{-1, 0, 1\}$ . These correspond to either a cell with orientation opposite to the chosen default one, a cell not part of the chain, or a cell with default orientation. In actual matrix calculations we directly use the coefficients as the column vector  $\mathbf{c} = (c^0 \ c^1 \ \dots \ c^s)^T$ .

Connectivity between volumes, faces, edges and points, is encoded in the boundary operator,  $\partial$ . The boundary operator is a linear map  $\partial : C(k) \mapsto C(k-1)$  defined as,

$$\partial c_{(k)} = \partial \left\{ c^j \cdot \sigma_{(k),j} \right\}_{j=0}^s = \left\{ c^j \cdot \partial \sigma_{(k),j} \right\}_{j=0}^s$$

The boundary  $\partial$  of a  $k$ -chain returns a unique  $(k-1)$ -chain and can be calculated as a linear combination of its  $k$ -cells boundaries. More precisely,  $\partial \sigma_{(k),j} = \left\{ e_j^i \sigma_{(k-1),i} \right\}_{i=0}^r$ , where  $e_j^i$  has the value,

1.  $e_j^i = 0$ , if  $\sigma_{(k-1),i}$  is not part of the boundary of  $\sigma_{(k),j}$ .
2.  $e_j^i = 1$ , if  $\sigma_{(k-1),i}$  is part of the boundary of  $\sigma_{(k),j}$  with compatible orientation.
3.  $e_j^i = -1$ , if  $\sigma_{(k-1),i}$  is part of the boundary of  $\sigma_{(k),j}$  with incompatible orientation

Figure 7 illustrated what we mean with compatible and incompatible orientation.

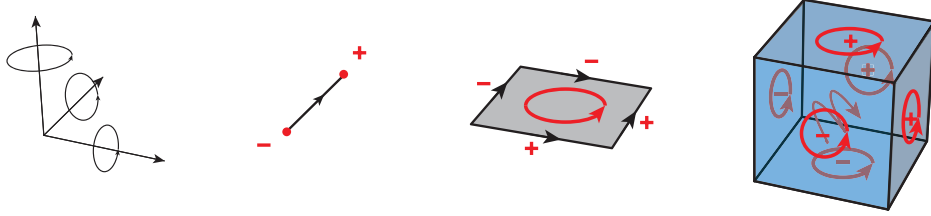


Figure 7: Compatible orientation (+) and incompatible orientation (-) between volumes and boundary faces, faces and boundary edges, edges and boundary points.

Hence,

$$\partial c_{(k)} = \left\{ c^j \cdot \partial \sigma_{(k),j} \right\}_{j=0}^s = \left\{ \sum_{j=0}^s c^j e_j^i \cdot \sigma_{(k-1),i} \right\}_{i=0}^r = \left\{ d^i \cdot \sigma_{(k-1),i} \right\}_{i=0}^r = d_{(k-1)}.$$

So the boundary of  $c_{(k)}$  is the unique  $(k-1)$ -chain,  $d_{(k-1)}$ , of which the coefficients are given by  $d^i = \sum_{j=0}^s c^j e_j^i$ . The action of the boundary operator therefore allows the matrix vector product  $\mathbf{d} = \mathbf{E}_{k-1,k} \mathbf{c}$ . Here  $\mathbf{E}_{k-1,k}$  is a rank  $(C_{(k-1)}) \times \text{rank}(C_{(k)})$  incidence matrix with coefficients  $(\mathbf{E}_{k-1,k})_{ij} = e_j^i$ . Note that in matrix calculations we only use the coefficients, not the basis chains. Example 3.1 shows the incidence matrices associated with the numbered and oriented cell complex of Figure 6b.

**Example 3.1 (Incidence matrices in  $\mathbb{R}^3$ ).** Consider the numbered and oriented cell complex in Figure 6b. The connectivity between points, edges, faces and volumes is encoded in the following incidence matrices.  $\mathbf{E}_{0,1}$  maps from 1-chains to 0-chains,  $\mathbf{E}_{1,2}$  maps from 2-chains to 1-chains and  $\mathbf{E}_{2,3}$  maps from 3-chains to 2-chains.

$$\mathbf{E}_{0,1} = \begin{bmatrix} -1 & 0 & 0 & 0 & 1 & 0 & 0 & 0 & -1 & 0 & 0 & 0 \\ 1 & 0 & 0 & 0 & 0 & 1 & 0 & 0 & 0 & -1 & 0 & 0 \\ 0 & -1 & 0 & 0 & -1 & 0 & 0 & 0 & 0 & 0 & -1 & 0 \\ 0 & 1 & 0 & 0 & 0 & -1 & 0 & 0 & 0 & 0 & 0 & -1 \\ 0 & 0 & -1 & 0 & 0 & 0 & 1 & 0 & 0 & 1 & 0 & 0 \\ 0 & 0 & 1 & 0 & 0 & 0 & 0 & 1 & 0 & -1 & 0 & 0 \\ 0 & 0 & 0 & -1 & 0 & 0 & -1 & 0 & 0 & 0 & 1 & 0 \\ 0 & 0 & 0 & 1 & 0 & 0 & 0 & -1 & 0 & 0 & 0 & 1 \end{bmatrix}, \quad \mathbf{E}_{1,2} = \begin{bmatrix} 0 & 0 & 0 & 1 & 1 & 0 \\ 0 & 0 & 1 & 0 & -1 & 0 \\ 0 & 0 & 0 & -1 & 0 & 1 \\ -1 & 0 & 0 & 0 & 1 & 0 \\ 0 & -1 & 0 & 0 & -1 & 0 \\ 1 & 0 & 0 & 0 & 0 & 1 \\ 0 & 1 & 0 & 0 & 0 & -1 \\ -1 & 0 & 0 & -1 & 0 & 0 \\ 0 & -1 & 0 & 1 & 0 & 0 \\ 1 & 0 & -1 & 0 & 0 & 0 \\ 0 & 1 & 1 & 0 & 0 & 0 \end{bmatrix}, \quad \mathbf{E}_{2,3} = \begin{bmatrix} -1 \\ 1 \\ -1 \\ 1 \\ -1 \\ 1 \end{bmatrix}$$

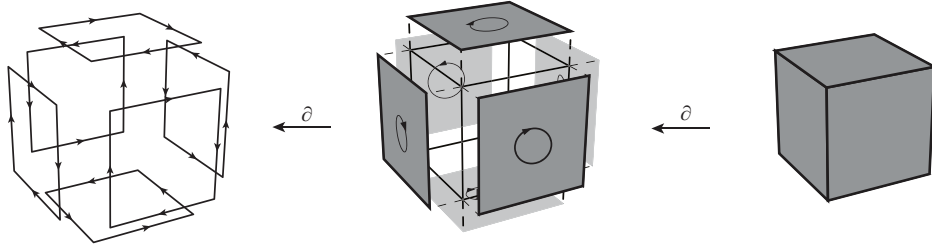


Figure 8: A double application of the boundary operator leads to an empty chain. Note that all edges are oriented in the opposite way, so any value associated with them cancels.

One can readily check that the boundary of the boundary is empty,

$$E_{0,1}E_{1,2} = (0 \quad \dots \quad 0)^T \quad \text{and} \quad E_{1,2}E_{2,3} = (0 \quad \dots \quad 0)^T$$

We now introduce the most important property of the boundary operator, which leads to some profound consequences in the description of geometry and physics. Picture for example a finite dimensional volume  $V$  in  $\mathbb{R}^3$ . It is clear that its bounding surface  $\partial V$  encloses all of  $V$  (this is in fact the definition of the boundary). This means that the surface  $\partial V$  has no boundary itself; it is boundaryless. Figure 8 illustrates that taking the boundary twice of a volume leads to an empty 1-chain.

In general, taking the boundary twice of a  $k$ -chain leads to an empty  $(k - 2)$ -chain,

$$\partial\partial c_{(k)} = 0_{(k-2)} \quad \text{for all } c_{(k)} \in C_{(k)}(D). \quad (19)$$

The set of  $k$ -chains and boundary operators thus gives rise to an exact sequence on contractible domains, the chain complex  $(C_{(k)}(D), \partial)$

$$\dots \xleftarrow{\partial} C_{(k-1)}(D) \xleftarrow{\partial} C_{(k)}(D) \xleftarrow{\partial} C_{(k+1)}(D) \xleftarrow{\partial} \dots \quad (20)$$

### 3.2. Cochains and the coboundary operator

So far we have learned how to calculate with discrete geometric objects, such as oriented points, edges, faces and volumes. By duality pairing with discrete geometry, we introduce cochains as discrete analogues of differential forms. Cochains can describe for instance integral values along a chain. Integration itself is however nothing but the 'measurement technique' that assigns global values to cells. For our purpose, it is most convenient to think of cochains in the most general way as any set of global values associated with oriented points, edges, faces and volumes in the mesh (cell complex). More clearly, they need not be integral values. This fact will allow us maximum freedom in the projection of differential forms - to be discussed in the next section - where we use cochains as degrees of freedom in combination with suitable basis functions based on NURBS.

A  $k$ -cochain is an expression which looks like,

$$a^{(k)} = \left\{ a_i \cdot \sigma^{(k),i} \right\}_{i=0}^s \quad \text{with } a_i \in \mathbb{R} \quad \text{and} \quad \sigma^{(k),i} \in C^{(k)}. \quad (21)$$

In contrast to chains, we use subscript for the coefficients  $a_i$  and superscript to denote the basis  $\sigma^{(k),i}$ . While we considered chains only with coefficients  $\{-1, 0, 1\}$ , we allow the coefficients of cochains to be any real number. As with chains, we shall use the coefficients directly as the column vector  $\mathbf{a} = (a_0 \quad a_1 \quad \dots \quad a_s)^T$  in matrix calculations.

Cochains are linear functionals on chains, and by choosing the basis cochains  $\sigma^{(k),i}$  dual to that of the space of chains,  $\langle \sigma^{(k),i}, \sigma_{(k),j} \rangle = \delta_{ij}^i$ , we can define the duality pairing between chains and cochains as,

$$\langle a^{(k)}, c_{(k)} \rangle := \sum_{i=0}^s a_i \cdot c^i = \mathbf{a}^T \mathbf{c} \in \mathbb{R} \quad (22)$$

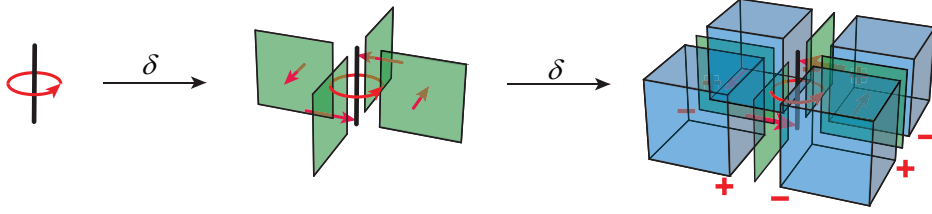


Figure 9: A double application of the coboundary operator leads to an empty cochain. Note that the two additions of face values per volume cancel each other out.

Note the similarity between duality pairing of differential forms and geometry by means of integration (6). In the discrete setting, integration is replaced by summation (22).

We can now define a discrete Stokes theorem, the mother of all equations, in terms of chains and cochains. As in the continuous setting where the exterior derivative is the formal adjoint of the boundary operator (8), we can define the coboundary operator on cochains as the formal adjoint of the boundary operator on chains,

$$\langle \delta b^{(k-1)}, c_{(k)} \rangle := \langle b^{(k-1)}, \partial c_{(k)} \rangle \quad (23)$$

for all  $b^{(k-1)} \in C_{(k-1)}(D)$  and  $c_{(k)} \in C_{(k)}(D)$ . While the boundary is a map,  $\partial : C_{(k)} \mapsto C_{(k-1)}$ , the coboundary is a map,  $\delta : C^{(k-1)} \mapsto C^{(k)}$ . Analogous to the exterior derivative  $d$  acting on forms in the continuous setting, the coboundary operator acts as a discrete derivative on cochains. The coboundary is thus a discrete version of the gradient ( $k = 1$ ), curl ( $k = 2$ ) and divergence ( $k = 3$ ) operators from vector calculus.

Earlier we remarked the fact that  $\partial \circ \partial = 0$ , has important consequences in physics. Amongst others, it implies that  $\delta \circ \delta = 0$ , see Figure 9. This is easily proven using (23) twice and (19),

$$\langle \delta \delta b^{(k-1)}, e_{(k+1)} \rangle \stackrel{(23)}{=} \langle \delta b^{(k-1)}, \partial e_{(k+1)} \rangle \stackrel{(23)}{=} \langle b^{(k-1)}, \partial \partial e_{(k+1)} \rangle \stackrel{(19)}{=} 0$$

This property is analogous to (12) and the important vector calculus identities  $\text{curl grad} = 0$  and  $\text{div curl} = 0$  in continuous space.

We can now set up the following exact sequence, known as a cochain complex  $(C^{(k)}(D), \delta)$ ,

$$\dots \xrightarrow{\delta} C^{(k-1)}(D) \xrightarrow{\delta} C^{(k)}(D) \xrightarrow{\delta} C^{(k+1)}(D) \xrightarrow{\delta} \dots \quad (24)$$

Since we have a matrix representation of the boundary operator, we can derive a matrix representation of the coboundary operator, using the adjoint property of the boundary and coboundary operator (23),

$$\langle b^{(k-1)}, \partial c_{(k)} \rangle \stackrel{(22)}{=} \mathbf{b}^T (\mathbf{E}_{k-1,k} \mathbf{c}) = (\mathbf{E}_{k-1,k}^T \mathbf{b})^T \mathbf{c} \stackrel{(22)}{=} \langle \delta b^{(k-1)}, c_{(k)} \rangle. \quad (25)$$

We can conclude that the matrix representation of the coboundary operator is given by  $\mathbf{D}_{k,k-1} = \mathbf{E}_{k-1,k}^T$ . We can therefore perform differentiation in the discrete setting using the matrix representation  $\mathbf{a} = \mathbf{D}_{k,k-1} \mathbf{b}$ . Furthermore,  $\mathbf{D}_{k+1,k} \mathbf{D}_{k,k-1} = \begin{pmatrix} 0 & \dots & 0 \end{pmatrix}^T$ , so the matrix representation of the gradient, curl and divergence exactly preserves the null space of the differential operators.

#### 4. Commuting projection

Balance equations, represented by the Generalized Stokes theorem (8), allow an exact discrete representation in terms of chains and cochains using (23). Since the structure of these equations is inherently discrete and metric free, we do not expect that basis functions play any role here. The constitutive equations - the material and metric dependent relations - on the other hand, require a continuous formulation of both the geometry and the field variables, and here is where the basis functions come in to play.

A continuous representation of field variables involves approximation by a suitable projection,  $\pi_h : \Lambda^k(\Omega) \mapsto \Lambda_h^k(\Omega)$ , from an infinite dimensional space  $\Lambda^k(\Omega)$  of differential forms, to a finite dimensional conforming subspace  $\Lambda_h^k(\Omega) \subset \Lambda^k(\Omega)$ . Approximation always involves a loss in information. It is however important that the error is bounded by a certain constant  $C < \infty$ ,

$$\text{approximation property: } \|a^k - \pi_h a^k\|_{\Lambda^k} \leq C \cdot h^p \quad \text{for all } a^k \in \Lambda^k(\Omega) \quad (26)$$

for a norm defined on  $\Lambda^k(\Omega)$ , where  $p$  denotes the approximation order and  $h$  is a measure of the the maximum partitioning size. In order to be consistent, the projection should reproduce all of  $\Lambda_h^k(\Omega)$ , which means that,

$$\text{consistency property: } \pi_h \circ \pi_h a^k = \pi_h a^k \quad \text{for all } a^k \in \Lambda^k(\Omega) \quad (27)$$

These two requirements are in general met by polynomial approximations. For interpolation estimates of for example NURBS and splines, see [33, 34] respectively.

To capture the behavior of a physical phenomena well, a discretization method should not only approximate the spaces of the infinite dimensional system, but should also follow the structure induced by the relations between them, i.e. the structure induced by the balance laws and constitutive equations (Figure 2). Only then will a discrete representation of the physics have any physical significance. The focus of this paper is to derive a projection of differential forms which commutes with differentiation,

$$\begin{array}{ccc} \Lambda^k(\Omega) & \xrightarrow{d} & \Lambda^{k+1}(\Omega) \\ \pi_h \downarrow & & \downarrow \pi_h \\ \Lambda_h^k(\Omega) & \xrightarrow{d} & \Lambda_h^{k+1}(\Omega) \end{array} \quad (28)$$

Projection and subsequent differentiation should give the same result as first applying the derivative and then do the projection. This commuting diagram property will guarantee that conservation and balance laws remain exactly satisfied in the discrete setting. Furthermore, this property is the key to naturally stable and consistent numerical algorithms. It can be shown that (28) implies a conforming Hodge decomposition, which together with the Poincaré inequality proves inf-sup stability. For more details we refer the reader to the papers by Kreeft et. al. [22, 23].

To assure that the balance laws are exactly satisfied, even on curved meshes, we require that the projection is independent of geometric transformations. This means that the projection should be constructed such that it commutes with the pull back as well,

$$\begin{array}{ccc} \Lambda^k(\Phi(\Omega')) & \xrightarrow{\Phi^*} & \Lambda^k(\Omega') \\ \pi_h \downarrow & & \downarrow \pi_h \\ \Lambda_h^k(\Phi(\Omega')) & \xrightarrow{\Phi^*} & \Lambda_h^k(\Omega') \end{array} \quad (29)$$

This can be achieved by constructing the projection such that it preserves the integrals of a differential  $k$ -form,  $a^k$ , along a chain  $c_{(k)}$ . Using the fact that the pull back  $\Phi^*$  is the adjoint of the map  $\Phi$  (7), we obtain the desired result,

$$\int_{c_{(k)}} \pi_h \Phi^* a^k = \int_{c_{(k)}} \Phi^* a^k = \int_{\Phi(c_{(k)})} a^k = \int_{\Phi(c_{(k)})} \pi_h a^k = \int_{c_{(k)}} \Phi^* \pi_h a^k. \quad (30)$$

#### 4.1. Reduction, change of bases and reconstruction

We extend the commuting diagram in (28) to define operations between the continuous (Section 2) and discrete formalism (Section 3). Following Bochev and Hyman [18], we introduce two separate operators, the reduction  $\mathcal{R}$  and reconstruction  $\mathcal{I}$  - which map differential forms to cochains and cochains to a finite dimensional representation of differential forms, respectively. Additionally we introduce a change of basis from cochains to a different type of cochains. As we shall see, this change of basis will allow maximum freedom in the choice of reconstruction method.

**Reduction**  $\mathcal{R} : \Lambda^k(\Omega) \mapsto C^{(k)}(D)$  is an abstraction of the measurement process and is given by the DeRahm map (31), which is defined by means of integration,

$$\langle \mathcal{R}(a^k), c_{(k)} \rangle = \int_{c_{(k)}} a^k. \quad (31)$$

To be able to use the coboundary as a discrete derivative, as outlined in Section 3, we require that the reduction commutes with differentiation,

$$\begin{array}{ccc} \Lambda^k(\Omega) & \xrightarrow{d} & \Lambda^{k+1}(\Omega) \\ \mathcal{R} \downarrow & & \downarrow \mathcal{R} \\ C^{(k)}(D) & \xrightarrow{\delta} & C^{(k+1)}(D) \end{array} \quad (32)$$

which is indeed the case as can be proven by using Stokes theorem and the duality between the boundary and coboundary operator,

$$\langle \mathcal{R}(da^k), c_{(k+1)} \rangle \stackrel{(31)}{=} \int_{c_{(k+1)}} da^k \stackrel{(8)}{=} \int_{\partial c_{(k+1)}} a^k \stackrel{(31)}{=} \langle \mathcal{R}(a^k), \partial c_{(k+1)} \rangle \stackrel{(23)}{=} \langle \delta \mathcal{R}(a^k), c_{(k+1)} \rangle$$

**Change of basis**  $\mathcal{F} : \bar{C}^{(k)}(D) \mapsto C^{(k)}(D)$  is an invertible map from a cochain  $\bar{a}^{(k)} = \{\bar{a}_j \cdot \bar{\sigma}^{(k),j}\}_{j=0}^s \in \bar{C}^{(k)}(D)$ , to a different type of cochain  $a^{(k)} = \{a_j \cdot \sigma^{(k),j}\}_{j=0}^s \in C^{(k)}(D)$  which are defined by means of integration (31). The change of basis  $\mathcal{F}$  makes it possible to use a much wider range of reconstruction methods. It provides the freedom to use degrees of freedom other than nodal values, curve, surface and volume integrals, while maintaining all the advantages of a compatible approach. For the reconstruction of 0-forms, for example, we no longer require nodal interpolants, but can use any basis that possesses partition of unity, for example NURBS. In practice, the change of basis is given by a square invertible matrix equivalent to that in an interpolation / histopolation problem.

Since  $\mathcal{F}$  is a map from cochains to cochains, we require that it commutes with discrete differentiation by means of the coboundary operator,

$$\begin{array}{ccc} C^{(k)}(D) & \xrightarrow{\delta} & C^{(k+1)}(D) \\ \mathcal{F}^{-1} \downarrow & & \downarrow \mathcal{F}^{-1} \\ \bar{C}^{(k)}(D) & \xrightarrow{\delta} & \bar{C}^{(k+1)}(D) \end{array} \quad (33)$$

The commuting diagram in (33) guarantees that the mathematical structure remains exactly the same after change of basis. The discrete modeling tools introduced in Section 3 therefore remain unaltered and we can perform discrete differentiation using the matrix representation  $D_{k+1,k} = E_{k,k+1}^T$ , as explained in the end of Section 3.

**Reconstruction**  $\mathcal{I} : \bar{C}^{(k)}(D) \mapsto \Lambda_h^k(\Omega)$  maps cochains  $\bar{a}^{(k)} = \{\bar{a}_j \cdot \bar{\sigma}^{(k),j}\}_{j=0}^s \in \bar{C}^{(k)}(D)$  back to a finite dimensional representation of a differential form  $a_h^k \in \Lambda_h^k(\Omega) \subset \Lambda^k(\Omega)$ . In order to use the discrete calculus introduced in Section 3 the reconstruction is required to commute with differentiation,

$$\begin{array}{ccc} \bar{C}^{(k)}(D) & \xrightarrow{\delta} & \bar{C}^{(k+1)}(D) \\ \mathcal{I} \downarrow & & \downarrow \mathcal{I} \\ \Lambda_h^k(\Omega) & \xrightarrow{d} & \Lambda_h^{k+1}(\Omega) \end{array} \quad (34)$$

This way we can perform the gradient, curl and divergence in the discrete setting, while continuous representations can be reconstructed where and whenever required.

The commuting property of projection with differentiation (28) can be seen as the composition of the commuting relations in (32), (33) and (34) and is illustrated in the following diagram,

$$\begin{array}{ccc}
 \Lambda^k(\Omega) & \xrightarrow{d} & \Lambda^{k+1}(\Omega) \\
 \mathcal{R} \downarrow & & \downarrow \mathcal{R} \\
 C^{(k)}(D) & \xrightarrow{\delta} & C^{(k+1)}(D) \\
 \mathcal{F}^{-1} \downarrow & & \downarrow \mathcal{F}^{-1} \\
 \bar{C}^{(k)}(D) & \xrightarrow{\delta} & \bar{C}^{(k+1)}(D) \\
 \mathcal{I} \downarrow & & \downarrow \mathcal{I} \\
 \Lambda_h^k(\Omega) & \xrightarrow{d} & \Lambda_h^{k+1}(\Omega)
 \end{array}
 \quad (35)$$

The choice of reconstruction,  $\mathcal{I} : \bar{C}^{(k)}(D) \mapsto \Lambda_h^k(\Omega)$ , uniquely defines that of  $\mathcal{I} : \bar{C}^{(k+1)}(D) \mapsto \Lambda_h^{k+1}(\Omega)$  through commutation with differentiation (34). This in practice means that we choose a basis for  $\Lambda_h^0(\Omega)$  and derive the remaining finite dimensional spaces of differential forms,  $\Lambda_h^k(\Omega)$ , for  $k = 1, \dots, n$ , using the commuting properties.

Furthermore, from (27) it naturally follows that the change of basis is related to the reduction and reconstruction by,  $\mathcal{F} := \mathcal{R} \circ \mathcal{I}$ . Therefore the choice of basis for 0-forms determines not only the basis for all other spaces of differential forms, but also uniquely defines the change of basis  $\mathcal{F} : \bar{C}^{(k)}(D) \mapsto C^{(k)}(D)$  for  $k = 0, 1, \dots, n$ .

We will study the commuting properties in (35) in more detail in the univariate case, see Figure 10. Once all spaces and operators are determined in the univariate case, we shall use the tensor product to develop multivariate spaces of discrete differential forms.

#### 4.2. Interpolation and histopolation

The commuting relations in (35) are graphically illustrated in Figure 10 in the case of 1D-space. Projection of a 0-form is equivalent to solving an interpolation problem where a set of data measurements are interpolated, while the projection of a 1-form is equivalent to solving a histopolation problem, where a set of line integrals are preserved in the projection.

Say we wish to approximate the 0-form in Figure 10, which represents for example a temperature field  $T(x)$ . We seek the finite dimensional approximation  $T_h(x) = \pi_h T(x)$  in the following space,

$$\Lambda_h^0(\Omega) := \left\{ \mathcal{I} \left\{ \bar{T}_j \cdot \bar{\sigma}^{(0),j} \right\}_{j=0}^n = \sum_{j=0}^n \bar{T}_j N_j(x), \text{ for all } \bar{T}_j \in \mathbb{R} \right\}, \quad (36)$$

where the degrees of freedom  $\bar{T}_j$  are the coefficients in the 0-cochain  $\{\bar{T}_j \cdot \bar{\sigma}^{(0),j}\}_{j=0}^n$  and the  $\{N_j(x)\}_{j=0}^n$  are linear independent basis functions that posses a partition of unity,  $\sum_{j=0}^n N_j(x) = 1$ .

The projection of a 0-form  $T_h(x) = \pi_h T(x)$  is required to follow  $\mathcal{R}(T(x)) = \mathcal{R}(T_h(x))$ , which means that  $T_h(x)$  interpolates  $T(x)$  at a chosen set of nodes  $\{x_i\}_{i=0}^n$ . Then, using (36), we can set up the  $n+1$  by  $n+1$  system of linear equations,

$$\pi_h T(x_i) = \sum_{j=0}^n \bar{T}_j N_j(x_i) = T(x_i) \quad \text{for } i = 0, 1, \dots, n \quad (37)$$

and find the unique set of coefficients  $\{\bar{T}_j\}_{j=0}^n$ . This system is guaranteed to have a solution when the matrix  $N$  with coefficients  $N_{ij} = N_j(x_i)$  is invertible, which is the case when  $x_i \in \text{span}\{N_i(x)\}$ , for  $i = 0, \dots, n$  [35]. Note that the change of basis  $\mathcal{F} = \mathcal{R} \circ \mathcal{I}$  is thus given by this square interpolation matrix  $N$ . The inverse map  $\mathcal{F}^{-1} = N^{-1}$ , depicted in the middle of the left hand side of Figure 10, is thus equivalent to solving the interpolation problem.

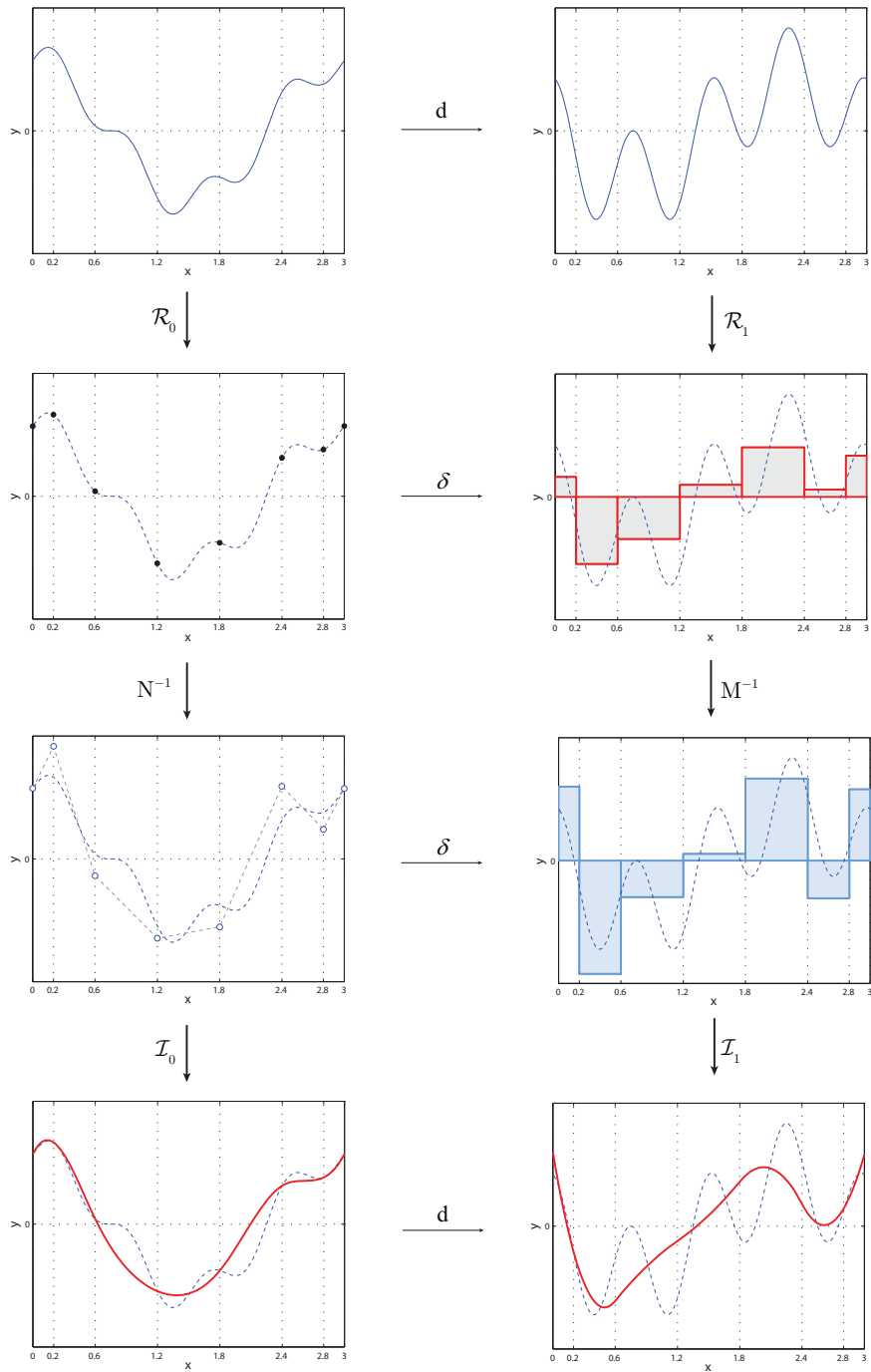


Figure 10: While a zero form is projected by interpolating a set of nodal values (left), its derivative (right) is projected by interpolating a set of integral values; a process called histopolation. This construction guarantees that the projection commutes with differentiation. Furthermore, the projection is broken down in three stages: 1) the reduction process  $\mathcal{R}$  reducing a 0-form and its derivative to a set of nodal and integral values, respectively; 2) A change of basis from nodal and integral values to new 'node' and 'edge' type of degrees of freedom. This change of basis is equivalent to solving an interpolation problem  $N^{-1}$  and histopolation problem  $M^{-1}$ , respectively. 3) the reconstruction process  $\mathcal{I}$  which is simply given by a linear combination of the new 'node' (0-cochain), or 'edge' (1-cochain) degrees of freedom with the appropriate basis functions  $\{N_i(x)\}_{i=0}^n$  and  $\{M_i(x)\}_{i=1}^n$  respectively. The resolution is purposely kept low to illustrate the concepts of reduction, change of basis and reconstruction.



If we would like to approximate the derivative of the temperature field, the 1-form  $u^1(x) = dT(x)$ , we require a basis for 1-forms,

$$\Lambda_h^1(\Omega) = \left\{ \mathcal{I} \left\{ \bar{u}_j \cdot \bar{\sigma}^{(1),j} \right\}_{j=1}^n = \sum_{j=1}^n \bar{u}_j M_j(x), \text{ for all } \bar{u}_j \in \mathbb{R} \right\} \quad (38)$$

where the degrees of freedom  $\bar{u}_j$  are the coefficients in the 1-cochain  $\left\{ \bar{u}_j \cdot \bar{\sigma}^{(1),j} \right\}_{j=1}^n$  and therefore the basis functions  $\left\{ M_j(x) \right\}_{j=1}^n$  can be associated with edges.

The projection of a 1-form  $u_h^1 = \pi_h u^1$  is required to follow  $\mathcal{R}(u^1) = \mathcal{R}(u_h^1)$ , which means that the approximation should preserve the line integrals of the 1-form  $u^1(x) = dT(x)$  along the edges  $e_i = [x_{i-1}, x_i]$ . We can therefore set up the following  $n$  by  $n$  system of linear equations,

$$\int_{e_i} \pi_h u^1 = \sum_{j=1}^n \bar{u}_j \int_{e_i} M_j(x) = \int_{e_i} u^1(x) = T(x_i) - T(x_{i-1}) \quad \text{for } i = 1, 2, \dots, n \quad (39)$$

This process (right side of Figure 10) is called histopolation, from interpolation of a histogram. In this case, the change of basis  $\mathcal{F} = \mathcal{R} \circ \mathcal{I}$ , is equal to the invertible histopolation matrix  $M$ , of which the coefficients are given by,

$$M_{ij} = \int_{e_i} M_j(x)$$

The inverse map  $\mathcal{F}^{-1} = M^{-1}$ , depicted in the middle of the right hand side of Figure 10, is thus equivalent to solving the histopolation problem.

### 4.3. Edge functions

The idea now is to choose a basis  $\{N_i(x)\}_{i=0}^n$  for 0-forms, and to derive the new edge type of basis functions  $\{M_i(x)\}_{i=1}^n$  by using the commuting properties in (34). Connectivity of edges  $e_i$  and points  $x_i$ ,  $\partial e_i = x_i - x_{i-1}$ , implies that we can apply discrete differentiation using the coboundary (23),  $\bar{u}_i = \bar{T}_i - \bar{T}_{i-1}$ , for  $i = 1, 2, \dots, n$ . Hence, every coefficient  $\bar{T}_i$  can be written as  $\bar{T}_i = \bar{T}_0 + \sum_{j=1}^i (\bar{T}_j - \bar{T}_{j-1}) = \bar{T}_0 + \sum_{j=1}^i \bar{u}_j$ .

Using this result in the projection of a zero form and applying the exterior derivative,

$$d\pi_h T(x) = d \sum_{i=0}^n \bar{T}_i N_i(x) = \bar{T}_0 d \sum_{i=0}^n N_i(x) + \sum_{i=0}^n \left( \sum_{j=1}^i \bar{u}_j \right) dN_i(x).$$

Partition of unity implies that,  $d \sum_{j=0}^n N_j(x) = 0$ ; hence the first term cancels. The second term can be rewritten such that we obtain a relation for the edge basis functions  $\{M_i(x)\}_{i=1}^n$ ,

$$\begin{aligned} d\pi_h T^0(x) &= \bar{u}_1 dN_1(x) + \{\bar{u}_1 + \bar{u}_2\} dN_2(x) + \dots \\ &= \{dN_1(x) + \dots + dN_n(x)\} \bar{u}_1 + \{dN_2(x) + \dots + dN_n(x)\} \bar{u}_2 + \dots = \sum_{i=1}^n \bar{u}_i \sum_{j=i}^n dN_j(x). \end{aligned}$$

By defining the edge basis functions  $\{M_i(x)\}_{i=1}^n$  as,

$$M_i(x) = \sum_{j=i}^n dN_j(x) = - \sum_{j=0}^{i-1} dN_j(x), \quad \text{for } i = 1, 2, \dots, n, \quad (40)$$

we have obtained the commuting projection,

$$d\pi_h T^0(x) = d \sum_{i=0}^n \bar{T}_i N_i(x) = \sum_{i=1}^n (\bar{T}_i - \bar{T}_{i-1}) M_i(x) = \sum_{i=1}^n \bar{u}_i M_i(x) = \pi_h d T^0(x). \quad (41)$$

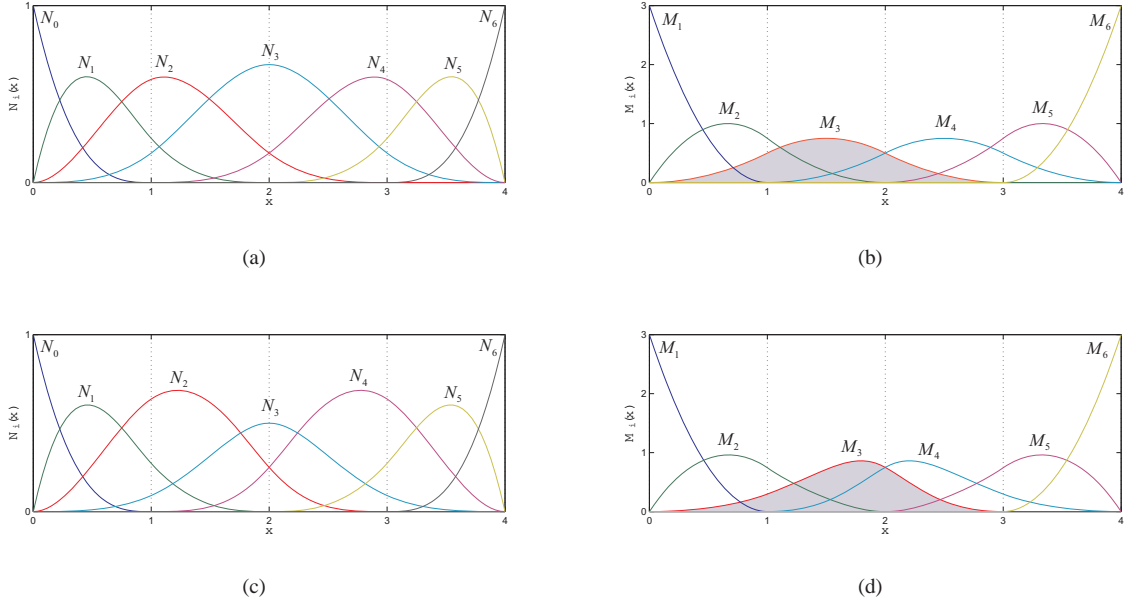


Figure 11: Cubic NURBS basis functions (left) and associated quadratic edge functions (right) corresponding to a knot vector  $\mathbf{t} = \{0, 0, 0, 0, 1, 2, 3, 4, 4, 4, 4\}$  under the influence of a different choice in weights. Every weight  $w_i$  associated with basis function  $N_i(x)$  is set equal to one, except  $w_3$ : Figure (a) and (b) correspond to  $w_3 = 1$  and thus simplify to B-splines; (c) and (d) correspond to  $w_3 = 1/2$ . Note that the 'node' NURBS basis features partition of unity  $\sum_{i=0}^n N_i(x) = 1$  on  $[0, 4]$ , while the edge functions feature unit integral  $\int_0^4 M_i(x) = 1$ .

As constructed, we can perform differentiation entirely independent from the basis functions. In fact, in  $dT_h^0 = \sum_{i=1}^n (\bar{T}_i - T_{i-1}) M_i(x) = \sum_{i=1}^n \bar{u}_i M_i(x) = u^1$ , the basis functions  $M_i(x)$  can be canceled out and we are left with discrete differentiation,  $\bar{u}_i = \bar{T}_i - T_{i-1}$  using the coboundary process as described in Section 3. The conservation laws thus become completely independent of the basis functions. This means that they are exactly satisfied, even on coarse and on arbitrary curved meshes, as already proven by the commutation property of the projection with the pullback (29).

While the set  $\{N_i\}_{i=0}^n$  sums up to 1 (partition of unity), the set of edge basis functions,  $\{M_i\}_{i=1}^n$ , scale such that they provide unit integral,

$$\bar{M}_i := \int_{x_0}^{x_n} M_i(x) = 1. \quad \text{for } i = 1, 2, \dots, n. \quad (42)$$

We proof this in the case that the set  $\{N_i(x)\}_{i=0}^n$  has interpolating end-conditions, i.e.  $T_h^0(x_0) = \sum_{i=0}^n \bar{T}_i N_i(x_0) = \bar{T}_0$  and  $T_h(x_n) = \sum_{i=0}^n \bar{T}_i N_i(x_n) = \bar{T}_n$ . Then we have by Stokes theorem (8),

$$\int_{x_0}^{x_n} dT_h^0(x) = \int_{x_0}^{x_n} \sum_{i=1}^n (\bar{T}_i - T_{i-1}) M_i(x) = \bar{T}_n \bar{M}_n + \sum_{i=1}^{n-1} \bar{T}_i (\bar{M}_i - \bar{M}_{i+1}) - \bar{T}_0 \bar{M}_1 = \bar{T}_n - \bar{T}_0.$$

Since this should hold for all  $\{\bar{T}_i \in \mathbb{R}\}_{i=0}^n$ ,  $\bar{M}_1 = \bar{M}_n = 1$  and consequently  $\{\bar{M}_i = 1\}_{i=1}^n$ .

Important is to realize that the derivation of the edge basis functions is valid for any basis  $\{N_i(x)\}_{i=0}^n$  (polynomial or non-polynomial) that is linear independent and is a partition of unity. Examples are Lagrange polynomials, Bezier, B-splines and NURBS. If the basis is nodal, which is the case for Lagrange polynomials, then the  $\bar{u}_i$  have geometric as well as physical meaning since they represent the line integrals along the mesh edges  $e_i$ . Edge functions based on Lagrange polynomials are used in the Mimetic framework presented in [20, 21, 22, 23]. In case of a non-nodal basis  $\{N_i(x)\}_{i=0}^n$ , such as Bezier polynomials, B-splines and NURBS, the degrees of freedom  $\bar{u}_i$  only have a geometric

interpretation, since they are discrete values associated with mesh edges  $e_i$ . They are however not related to differential forms by means of integration.

Compatible spaces of B-splines have already been used in [1, 13, 14, 16]. They make use of the fact that the derivative of a B-spline of order  $p$  is a B-spline of order  $p - 1$  and can be written in the following form [35],

$$d \sum_{i=0}^n \bar{T}_i B_{i,p}(x) = \sum_{i=1}^n (\bar{T}_i - \bar{T}_{i-1}) c_i \cdot B_{i,p-1}(x), \quad (43)$$

where the  $c_i$  are constants that depend on  $p$ , and the regularity of the mesh. We can directly observe that using B-splines, the 'node' functions,  $N_i(x)$ , are given by  $N_i(x) = B_{i,p}(x)$ , while the 'edge' functions,  $M_i(x)$ , are given by  $M_i(x) = c_i \cdot B_{i,p-1}(x)$ . The latter are called Curry Schoenberg B-splines, which was in fact the initial B-spline representation derived by Schoenberg [36]. It was later that B-splines were scaled to form a partition of unity.

In this paper we derive compatible spaces of discrete differential forms from NURBS [37], non-uniform rational B-splines. NURBS are rational functions of B-splines and are given as,

$$N_i(x) = \frac{w_i \cdot B_{i,p}(x)}{\sum_{i=0}^n w_i \cdot B_{i,p}(x)}. \quad (44)$$

NURBS trivially satisfy the required partition of unity, and can therefore be used as a basis to derive compatible spaces of discrete differential forms. Figure 11 shows an example of cubic NURBS basis functions and their corresponding edge functions for different choices of the NURBS weights  $w_i$ .

#### 4.4. Multivariate discrete differential forms

A basis for differential forms in  $n$ -dimensional space is simply obtained by means of the tensor product of the derived univariate 'node' and 'edge' functions. A basis for 2-forms in 2D is for example obtained by applying the tensor product of edge functions in both directions. We can define the following finite dimensional approximation spaces for 0-, 1-, and 2-forms in  $\mathbb{R}^2$ ,

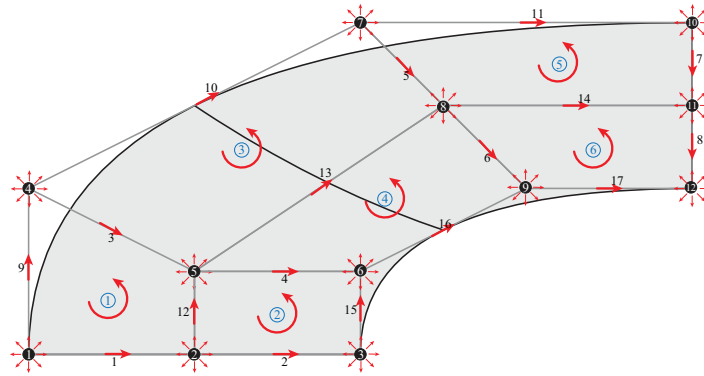
$$\begin{aligned} \Lambda_h^0(\Omega) &= \text{span} \left\{ N_i(x^1) \otimes N_j(x^2) \right\}_{i=0, j=0}^{n_1, n_2} \\ \Lambda_h^1(\Omega) &= \text{span} \left\{ M_i(x^1) \otimes N_j(x^2) \right\}_{i=1, j=0}^{n_1, n_2} \times \text{span} \left\{ N_i(x^1) \otimes M_j(x^2) \right\}_{i=0, j=1}^{n_1, n_2} \\ \Lambda_h^2(\Omega) &= \text{span} \left\{ M_i(x^1) \otimes M_j(x^2) \right\}_{i=1, j=1}^{n_1, n_2} \end{aligned}$$

Examples of 2-dimensional basis functions associated with inner and outer oriented points, edges, and faces are displayed in Figure 12 and 13. These spaces follow the following sequence, which is exact on contractible domains.

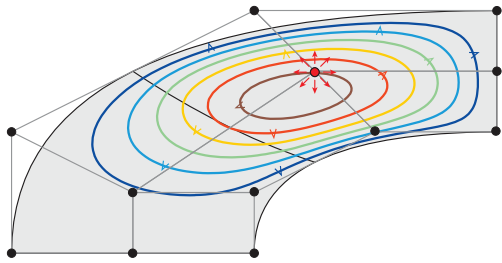
$$\begin{array}{ccccc} \Lambda^0(\Omega) & \xrightarrow{d} & \Lambda^1(\Omega) & \xrightarrow{d} & \Lambda^2(\Omega) \\ \pi_h \downarrow & & \pi_h \downarrow & & \pi_h \downarrow \\ \Lambda_h^0(\Omega) & \xrightarrow{d} & \Lambda_h^1(\Omega) & \xrightarrow{d} & \Lambda_h^2(\Omega) \end{array} \quad (45)$$

We will more deeply discuss the discrete spaces of differential forms in  $\mathbb{R}^3$  to stay close to our discussion in section 1. We introduce the following notation for 3-dimensional tensor product basis functions,

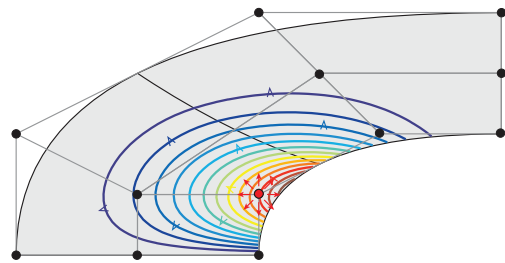
$$\begin{aligned} B_{i,j,k}(\mathbf{x}) &= N_i(x^1)N_j(x^2)N_k(x^3) \\ B_{i,j,k}^{(1)}(\mathbf{x}) &= M_i(x^1)N_j(x^2)N_k(x^3), & B_{i,j,k}^{(2)}(\mathbf{x}) &= N_i(x^1)M_j(x^2)N_k(x^3), & B_{i,j,k}^{(3)}(\mathbf{x}) &= N_i(x^1)N_j(x^2)M_k(x^3) \\ B_{i,j,k}^{(2,3)}(\mathbf{x}) &= N_i(x^1)M_j(x^2)M_k(x^3), & B_{i,j,k}^{(3,1)}(\mathbf{x}) &= M_i(x^1)N_j(x^2)M_k(x^3), & B_{i,j,k}^{(1,2)}(\mathbf{x}) &= M_i(x^1)M_j(x^2)N_k(x^3) \\ B_{i,j,k}^{(1,2,3)}(\mathbf{x}) &= M_i(x^1)M_j(x^2)M_k(x^3) \end{aligned}$$



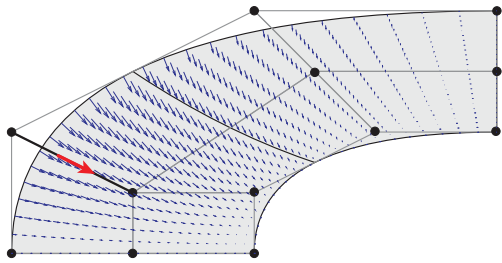
(a) Inner oriented cell complex



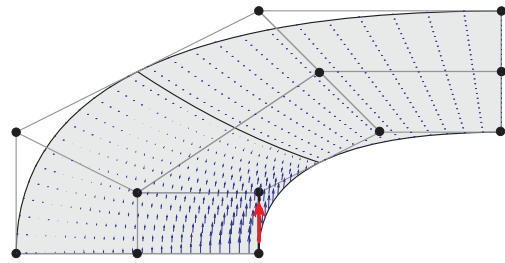
(b) Inner oriented 'node' function



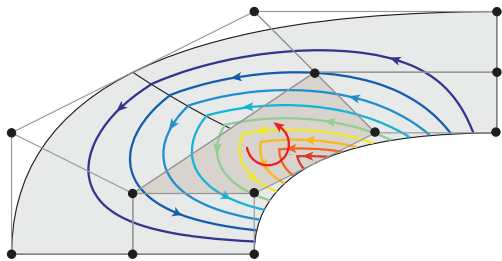
(c) Inner oriented 'node' function



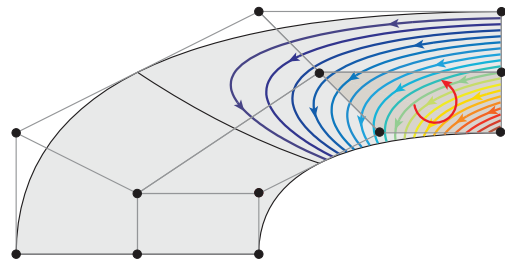
(d) Inner oriented 'edge' function



(e) Inner oriented 'edge' function

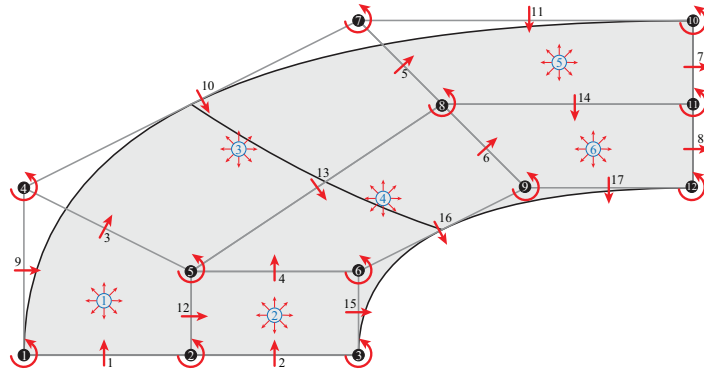


(f) Inner oriented 'face' function

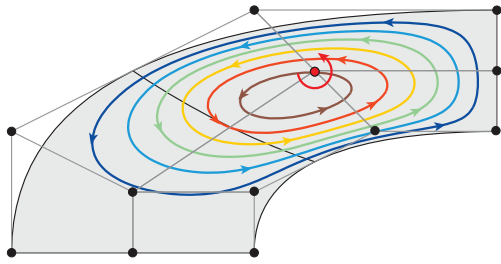


(g) Inner oriented 'face' function

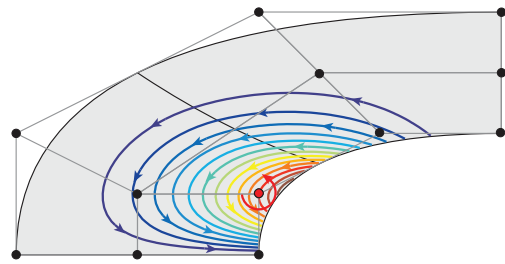
Figure 12: 2D examples of inner oriented 'node' (b and c), 'edge' (d and e) and 'face' (f and g) basis functions. The basis functions are derived from NURBS of bi-degree 2 and knot vectors  $U_1 = \{ 0, 0, 0, 1, 1, 1 \}$  and  $U_2 = \{ 0, 0, 0, 0.5, 1, 1, 1 \}$  with weights equal to 1 (NURBS reduces to B-spline).



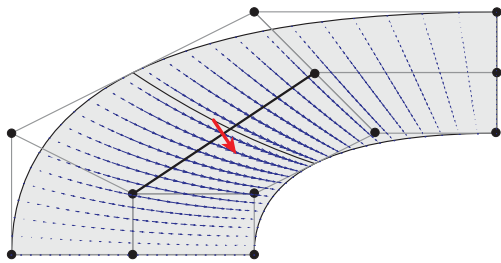
(a) Outer oriented cell complex



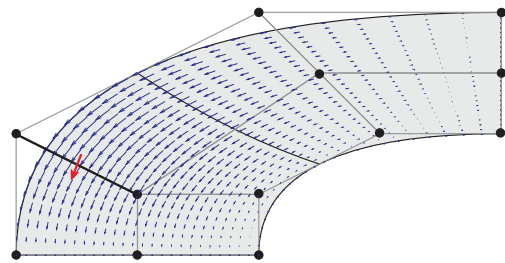
(b) Outer oriented 'node' function



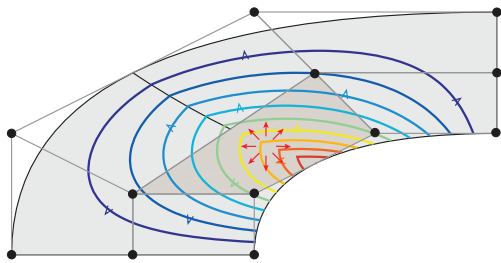
(c) Outer oriented 'node' function



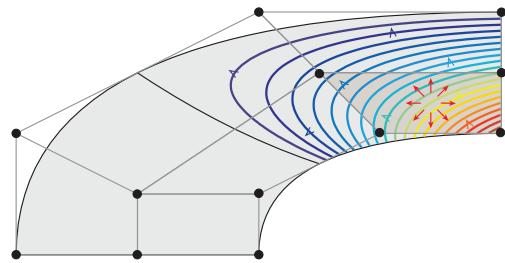
(d) Outer oriented 'edge' function



(e) Outer oriented 'edge' function



(f) Outer oriented 'face' function



(g) Outer oriented 'face' function

Figure 13: 2D examples of outer oriented 'node' (b and c), 'edge' (d and e) and 'face' (f and g) basis functions. The basis functions are derived from NURBS of bi-degree 2 and knot vectors  $U_1 = \{ 0, 0, 0, 1, 1, 1 \}$   $U_2 = \{ 0, 0, 0, 0.5, 1, 1, 1 \}$  with weights equal to 1 (NURBS reduces to B-spline).

Note that the superscripts indicate in which direction an edge function is used. We can then define the following finite dimensional approximation spaces for 0-, 1-, 2- and 3-forms,

$$\begin{aligned}
\Lambda_h^0(\Omega) &= \text{span} \left\{ B_{i,j,k}(\mathbf{x}) \right\}_{i=0,j=0,k=0}^{n_1,n_2,n_3} \\
\Lambda_h^1(\Omega) &= \text{span} \left\{ B_{i,j,k}^{(1)}(\mathbf{x}) \right\}_{i=1,j=0,k=0}^{n_1,n_2,n_3} \times \text{span} \left\{ B_{i,j,k}^{(2)}(\mathbf{x}) \right\}_{i=0,j=1,k=0}^{n_1,n_2,n_3} \times \text{span} \left\{ B_{i,j,k}^{(3)}(\mathbf{x}) \right\}_{i=0,j=0,k=1}^{n_1,n_2,n_3} \\
\Lambda_h^2(\Omega) &= \text{span} \left\{ B_{i,j,k}^{(2,3)}(\mathbf{x}) \right\}_{i=0,j=1,k=1}^{n_1,n_2,n_3} \times \text{span} \left\{ B_{i,j,k}^{(3,1)}(\mathbf{x}) \right\}_{i=1,j=0,k=1}^{n_1,n_2,n_3} \times \text{span} \left\{ B_{i,j,k}^{(1,2)}(\mathbf{x}) \right\}_{i=1,j=1,k=0}^{n_1,n_2,n_3} \\
\Lambda_h^3(\Omega) &= \text{span} \left\{ B_{i,j,k}^{(1,2,3)}(\mathbf{x}) \right\}_{i=1,j=1,k=1}^{n_1,n_2,n_3}
\end{aligned}$$

These spaces are constructed such that they satisfy the following sequence, which is exact on contractible domains,

$$\begin{array}{ccccccc}
\Lambda^0(\Omega) & \xrightarrow[\text{grad}]{d} & \Lambda^1(\Omega) & \xrightarrow[\text{curl}]{d} & \Lambda^2(\Omega) & \xrightarrow[\text{div}]{d} & \Lambda^3(\Omega) \\
\downarrow \pi_h & & \downarrow \pi_h & & \downarrow \pi_h & & \downarrow \pi_h \\
\Lambda_h^0(\Omega) & \xrightarrow[\text{grad}]{d} & \Lambda_h^1(\Omega) & \xrightarrow[\text{curl}]{d} & \Lambda_h^2(\Omega) & \xrightarrow[\text{div}]{d} & \Lambda_h^3(\Omega)
\end{array} \tag{46}$$

We emphasize that 0- and 3-forms are scalar valued functions and 1- and 2-forms are vector valued functions. Some examples of quantities such as temperature, velocity, vorticity and density are displayed in the following example.

**Example 4.1 (Reconstruction in  $R^3$ ).** *Examples of the finite dimensional reconstructions of 0-, 1-, 2- and 3-form fields.*

$$\begin{aligned}
0\text{-form: } T_h^{(0)}(\mathbf{x}) &= \sum_{i,j,k} \bar{T}_{i,j,k} B_{i,j,k}(\mathbf{x}) \\
1\text{-form: } u_h^{(1)}(\mathbf{x}) &= \sum_{i,j,k} \bar{u}_{i,j,k}^{(1)} B_{i,j,k}^{(1)}(\mathbf{x}) + \sum_{i,j,k} \bar{u}_{i,j,k}^{(2)} B_{i,j,k}^{(2)}(\mathbf{x}) + \sum_{i,j,k} \bar{u}_{i,j,k}^{(3)} B_{i,j,k}^{(3)}(\mathbf{x}) \\
2\text{-form: } \omega_h^{(2)}(\mathbf{x}) &= \sum_{i,j,k} \bar{\omega}_{i,j,k}^{(1)} B_{i,j,k}^{(2,3)}(\mathbf{x}) + \sum_{i,j,k} \bar{\omega}_{i,j,k}^{(2)} B_{i,j,k}^{(3,1)}(\mathbf{x}) + \sum_{i,j,k} \bar{\omega}_{i,j,k}^{(3)} B_{i,j,k}^{(1,2)}(\mathbf{x}) \\
3\text{-form: } f_h^{(3)}(\mathbf{x}) &= \sum_{i,j,k} \bar{f}_{i,j,k} B_{i,j,k}^{(1,2,3)}(\mathbf{x})
\end{aligned}$$

As in univariate space, the balance laws are completely independent of the basis functions and we can perform differentiation discretely. We thus have a discrete matrix representation of the gradient, curl and divergence operator which is exact, even on curved and coarse meshes, see Section 3. These relations hold for Lagrange, Bezier, B-spline, NURBS or any other basis  $\{N_i(x)\}_{i=0}^n$  that forms a partition of unity. This means that these relations hold independent of a specific numerical method.

**Example 4.2 (Discrete gradient operator).** *Consider  $u_h^1(\mathbf{x}) = \text{grad } T_h^0(\mathbf{x})$  where  $u_h^1(\mathbf{x})$  and  $T_h^0(\mathbf{x})$  are of the form as in example 4.1. Then the degrees of freedom  $\bar{u}_{i,j,k}^{(d)}$ , where  $d = 1, 2, 3$  represents component direction, are associated with edges and are given by,*

$$\bar{u}_{i,j,k}^{(1)} = \bar{T}_{i,j,k} - \bar{T}_{i-1,j,k}, \quad \bar{u}_{i,j,k}^{(2)} = \bar{T}_{i,j,k} - \bar{T}_{i,j-1,k} \quad \text{and} \quad \bar{u}_{i,j,k}^{(3)} = \bar{T}_{i,j,k} - \bar{T}_{i,j,k-1}$$

*This discrete representation allows a matrix vector product  $\mathbf{u} = D_{1,0} \mathbf{T}$  where  $D_{1,0} = E_{0,1}^T$  is an incidence matrix, see Example 3.1. This discrete gradient is exact and does not depend on geometric transformations, as proven in (29).*

**Example 4.3 (Discrete curl operator).** Consider  $\omega_h^2(\mathbf{x}) = \text{curl } u_h^1(\mathbf{x})$  where  $\omega_h^2(\mathbf{x})$  and  $u_h^1(\mathbf{x})$  are of the form as in example 4.1. Then the degrees of freedom  $\bar{\omega}_{i,j,k}^{(d)}$  are associated with faces and are given by,

$$\begin{aligned}\bar{\omega}_{i,j,k}^{(1)} &= \bar{u}_{i,j,k}^{(3)} - \bar{u}_{i,j-1,k}^{(3)} + \bar{u}_{i,j,k-1}^{(2)} - \bar{u}_{i,j,k}^{(2)} \\ \bar{\omega}_{i,j,k}^{(2)} &= \bar{u}_{i,j,k}^{(1)} - \bar{u}_{i,j,k-1}^{(1)} + \bar{u}_{i-1,j,k}^{(3)} - \bar{u}_{i,j,k}^{(3)} \\ \bar{\omega}_{i,j,k}^{(3)} &= \bar{u}_{i,j,k}^{(2)} - \bar{u}_{i-1,j,k}^{(2)} + \bar{u}_{i,j-1,k}^{(1)} - \bar{u}_{i,j,k}^{(1)}\end{aligned}$$

which allows a matrix vector product  $\boldsymbol{\omega} = \mathbf{D}_{2,1} \mathbf{u}$  where  $\mathbf{D}_{2,1} = \mathbf{E}_{1,2}^T$  is an incidence matrix, see Example 3.1. This discrete curl is exact and does not depend on geometric transformations, as proven in (29).

**Example 4.4 (Discrete divergence operator).** Consider  $f_h^3(\mathbf{x}) = \text{div } \omega_h^2(\mathbf{x})$  where  $\omega_h^2(\mathbf{x})$  and  $f_h^3(\mathbf{x})$  are of the form as in example 4.1. Then the degrees of freedom  $\bar{f}_{i,j,k}$  are associated with volumes and follow the discrete relation,

$$\bar{f}_{i,j,k} = \bar{\omega}_{i,j,k}^{(1)} - \bar{\omega}_{i-1,j,k}^{(1)} + \bar{\omega}_{i,j,k}^{(2)} - \bar{\omega}_{i,j-1,k}^{(2)} + \bar{\omega}_{i,j,k}^{(3)} - \bar{\omega}_{i,j,k-1}^{(3)}$$

which allows a matrix vector product  $\mathbf{f} = \mathbf{D}_{3,2} \boldsymbol{\omega}$  where  $\mathbf{D}_{3,2} = \mathbf{E}_{2,3}^T$  is an incidence matrix, see Example 3.1. This discrete divergence is exact and does not depend on geometric transformations, as proven in (29).

To summarize, with the appropriate basis functions in which to represent continuous differentiation,  $\beta_h^k(\mathbf{x}) = d \alpha_h^{k-1}(\mathbf{x})$  ( $k = 1, 2, 3$ ), the gradient, curl and divergence reduce to a relation between the expansion coefficients.

## 5. Mixed formulation for Stokes flow in terms of differential forms

In this section we will use the finite dimensional spaces of differential forms, developed in the previous section, in a mixed continuous Galerkin setting. We will apply the method to several 2D test problems concerning Stokes flow (see section 1). Which mixed formulation we choose to attack the problem, will solely dependent on physical considerations. Following the reasoning in section 1, we choose all variables as outer oriented differential forms, such that we can apply the topological divergence for mass conservation, see Figure 3. This ultimately results in a point-wise divergence free velocity field in the discrete setting. Furthermore, choosing all variables as outer oriented differential forms, has the advantage that normal velocity is prescribed in a strong sense, while tangential velocity is prescribed in a weak sense.

Consider an  $n$ -dimensional domain  $\Omega$ , filled with an incompressible fluid with constant viscosity  $\nu$ . Under these assumptions, Stokes flow can be described in terms of differential forms as,

$$d^* u^{n-1} = \omega^{n-2}, \quad d \omega^{n-2} + d^* p^n = f^{n-1}, \quad d u^{n-1} = 0 \quad (47)$$

Here velocity is an outer oriented  $(n-1)$ -form,  $u^{n-1}$ , pressure is an outer oriented  $n$ -form,  $p^n$ , the vorticity is an outer oriented  $(n-2)$ -form and the right-hand-side is an outer oriented  $(n-1)$ -form,  $f^{n-1}$ .

We follow the same reasoning as in [21] and derive the mixed formulation of the Stokes problem in 2 steps,

1. Multiply the equations in (47) by test functions  $\alpha^{n-2}$ ,  $\beta^{n-1}$  and  $\gamma^n$  to obtain  $L^2$  inner products terms.
2. Use integration by parts to replace the coderivative  $d^*$  by the exterior derivative  $d$  and an additional boundary integral using (16).

The Stokes problem can now be posed as follows: find  $\{\omega^{n-2} \in \Lambda^{n-2}, u^{n-1} \in \Lambda^{n-1}, p^n \in \Lambda^n\}$  for all  $\{\alpha^{n-2} \in \Lambda^{n-2}, \beta^{n-1} \in \Lambda^{n-1}, \gamma^n \in \Lambda^n\}$ , such that

$$(d \alpha^{n-2}, u^{n-1})_\Omega - (\alpha^{n-2}, \omega^{n-2})_\Omega = \int_{\partial\Omega} \alpha^{n-2} \wedge \star u^{n-1} \quad (48)$$

$$(\beta^{n-1}, d \omega^{n-2})_\Omega + (d \beta^{n-1}, p^n)_\Omega - \int_{\partial\Omega} \beta^{n-1} \wedge \star p^n = (\beta^{n-1}, f^{n-1})_\Omega \quad (49)$$

$$(\gamma^n, d u^{n-1})_\Omega = 0. \quad (50)$$

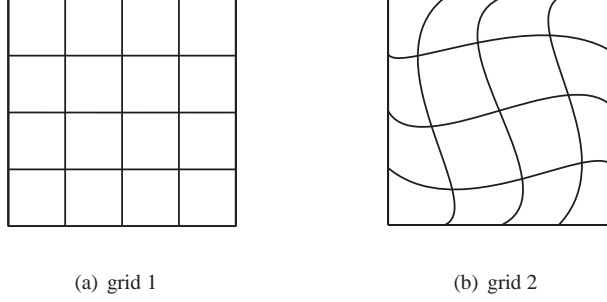


Figure 14: The Cartesian and curved mesh used in the convergence study.

This is the vorticity-velocity-pressure (VVP) formulation also used in [17, 21, 22, 38] which is well posed [22, 39]. In the discrete problem we merely replace the infinite dimensional spaces of differential forms by  $\{\omega_h^{n-2} \in \Lambda_h^{n-2}, u_h^{n-1} \in \Lambda_h^{n-1}, p_h^n \in \Lambda_h^n\}$ . Because,  $\Lambda_h(\Omega) \subset \Lambda(\Omega)$ , the discrete problem is automatically well posed as well. The problem is closed by imposing normal and tangential velocity components at the boundary. See [21, 22] for an overview of all admissible boundary conditions. The resulting system is symmetric and given by,

$$\begin{pmatrix} -M_{n-2} & D_{n-1,n-2}^T M_{n-1} & \emptyset \\ M_{n-1} D_{n-1,n-2} & \emptyset & D_{n,n-1}^T M_n - B_2(\mathbf{p}) \\ \emptyset & M_n D_{n,n-1} & \emptyset \end{pmatrix} \begin{pmatrix} \omega \\ \mathbf{u} \\ \mathbf{p} \end{pmatrix} = \begin{pmatrix} B_1(u^{n-1}) \\ M_{n-1}(f^{n-1}) \\ \emptyset \end{pmatrix} \quad (51)$$

The discrete curl  $D_{n-1,n-2} = E_{n-2,n-1}^T$  and divergence  $D_{n,n-1} = E_{n-1,n}^T$  are incidence matrices, see Section 3, depending solely on mesh topology and are exact irrespective of the geometry mapping  $\Phi$  and coarseness of the mesh. The inner product matrices  $M_{n-2}$ ,  $M_{n-1}$  and  $M_n$  are calculated by pulling the finite dimensional spaces of differential forms back to the reference domain  $\Omega'$  (section 2) and performing Gauss numerical integration there.  $B_1(u^{n-1})$  and  $B_2(\mathbf{p})$  represent the natural boundary terms, tangential velocity and tangential pressure, that arise due to integration by parts using (16). Since the tangential velocity is weakly enforced, it appears in the right hand side, while the pressure term  $B_2$  is not enforced and thus remains in the left hand side.

## 6. Numerical results

We will test the method on several common numerical test cases: 1) We compare with an analytical solution (same test problem as in [21]) and show results for  $h$ -refinement on a Cartesian and skewed, non-linear mesh; 2) Taylor Couette flow and compare with the analytical solution; and 3) lid driven cavity flow and compare with benchmark results of [40].

### 6.1. Manufactured solution

Consider as computational domain the unit square,  $\Omega = [0, 1]^2$ , filled with an incompressible fluid of viscosity,  $\nu = 1$ . As an analytical solution we choose,

$$\begin{aligned} \omega^0(x, y) &= -4\pi \sin(2\pi x) \sin(2\pi y). \\ u^1(x, y) &= -\sin(2\pi x) \cos(2\pi y) \cdot dy - \cos(2\pi x) \sin(2\pi y) \cdot dx \\ p^2(x, y) &= \sin(\pi x) \sin(\pi y) \cdot dx \, dy. \\ f^1(x, y) &= \left( -8\pi^2 \sin(2\pi x) \cos(2\pi y) + \pi \cos(\pi x) \sin(\pi y) \right) \cdot dy + \\ &\quad \left( -8\pi^2 \cos(2\pi x) \sin(2\pi y) - \pi \sin(\pi x) \cos(\pi y) \right) \cdot dx. \end{aligned}$$

We perform calculations on a Cartesian mesh as well as on a bicubic degree curved mesh, see Figure 14.



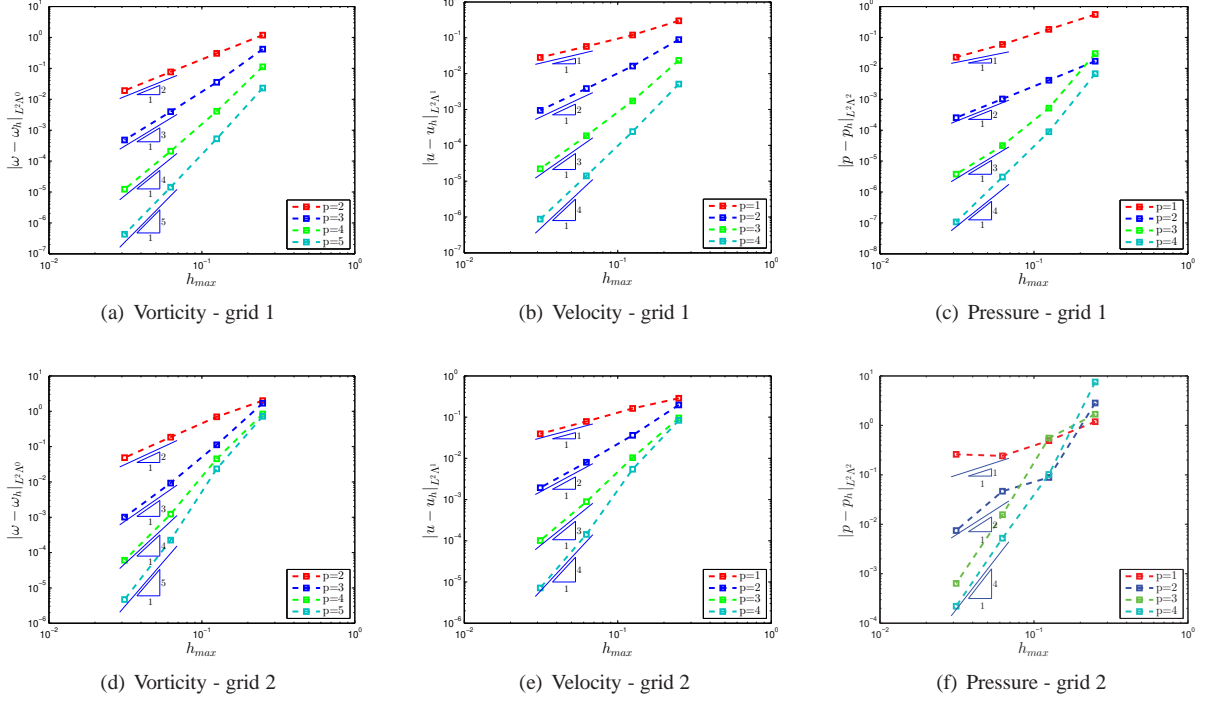


Figure 15: H-convergence for vorticity, velocity and pressure on grid 1 (a,b,c) and 2 (d,e,f).

The divergence of  $u_h^1$  is point wise zero at all stages of refinement. Figure 15 shows the convergence behavior under  $h$ -refinement of the vorticity, velocity and pressure for polynomial orders ranging from  $p = 2$  to  $p = 5$  for the vorticity and  $p = 1$  to  $p = 4$  for the velocity and pressure. The maximum mesh-size  $h_{max}$  is calculated as the maximum diagonal length of all elements divided by the square root of 2. We can observe optimal order of convergence for all variables on both grids. Only the pressure on grid 2 of polynomial order  $p = 1$  shows some odd behavior. This is probably due to the low order of approximation of the variables in conjunction with a higher order ( $p = 4$ ) non linear mapping of the geometry (super-parametric).

## 6.2. Taylor Couette flow

We consider a somewhat more realistic problem with an incompressible fluid with viscosity,  $\nu = 1$ , in a domain bounded by two contra rotating cylinders. The outer cylinder with radius  $r_{out} = 2$  is fixed, while the inner cylinder with radius  $r_{in} = 1$  rotates in counter clockwise direction with an angular velocity equal to 1.

The flow field in Cartesian coordinates  $(x,y)$  as a function of radius  $r$  is then described by the following velocity field,

$$u^1(r) = \left( -\frac{1}{3}r + \frac{4}{3r} \right) (-\sin \theta dy + \cos \theta dx) \quad (52)$$

and is depicted in Figure 16a.

The geometry is exactly represented by 4  $C^0$  NURBS patches of degree 2 by 1. Note that this test-case is more interesting since not all weights are equal to one. The weights associated with the four inner and four outer corners of the domain have weights equal to  $0.5 \cdot \sqrt{2}$ . Figure 16b shows optimal convergence of the velocity under  $h$ -refinement for polynomial orders of  $p = 1$  to  $p = 4$  in the radial direction. The pressure is constant throughout the domain and is up to machine precision at all stages of refinement. Here  $h_{max}$  represents the mesh-size in radial direction.

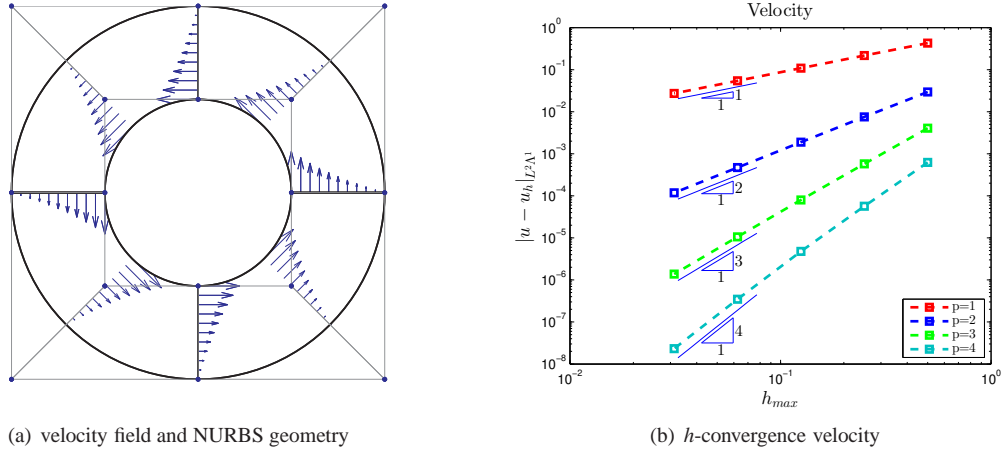


Figure 16: Flow field and NURBS geometry representation (a) using 4  $C^0$  patches; and  $h$ -convergence for velocity (b).

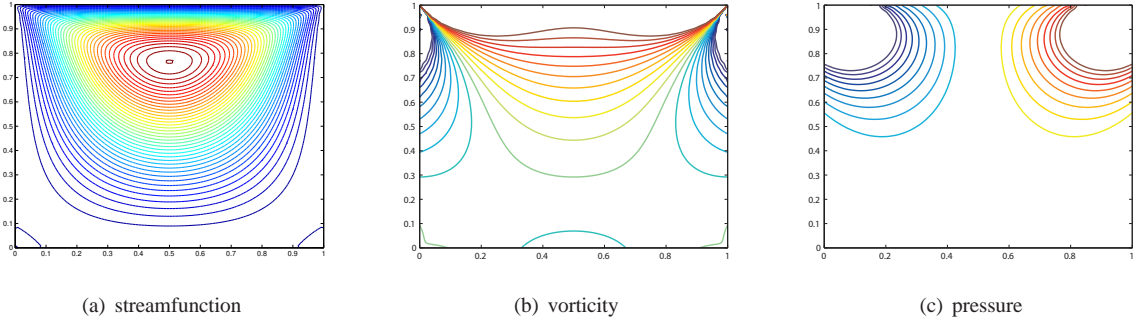


Figure 17: Results lid driven cavity flow on a 60x60 uniform bi-cubic NURBS mesh (weights are all equal to one) of highest regularity.

### 6.3. Lid driven cavity flow

The lid driven cavity flow is one of the classical benchmark cases to assess numerical methods and to verify Navier Stokes codes. Consider the unit square domain  $\Omega = [0, 1]^2$  filled with an incompressible fluid of viscosity  $\nu = 1$ . On the top of the domain we apply a tangential velocity  $u(x, 1) = 1$  while on the other sides of the domain the tangential velocity is set to zero. The result is a clockwise rotating flow with small counter rotating eddies in the two lower corners. Because of the discontinuity of the velocity in the two upper corners, both the vorticity and pressure are infinite at these places. These singularities make the lid driven cavity flow a challenging test case.

Figure 17 shows results for the stream function, vorticity and pressure on a bi-cubic uniform grid of maximum regularity and 60x60 degrees of freedom. We note that the divergence of velocity is point-wise zero in whole  $\Omega$ . Furthermore no special treatment has been given to the corner singularities.

In Figure 18 the horizontal component of velocity has been plotted along the vertical centerline  $(0.5, y)$  and the vertical component of velocity has been plotted along the horizontal centerline  $(y, 0.5)$ . The results confirm very well with the benchmark results of [40] even though the mesh is very coarse (9x9 uniform grid of polynomial order 1, 3 and 5). The most striking result is, however, that of the low order approximation. Note that although there is a clear point-wise difference, the integral values seem to match very well. This is a direct consequence of the conservation properties that we have build into the basis.

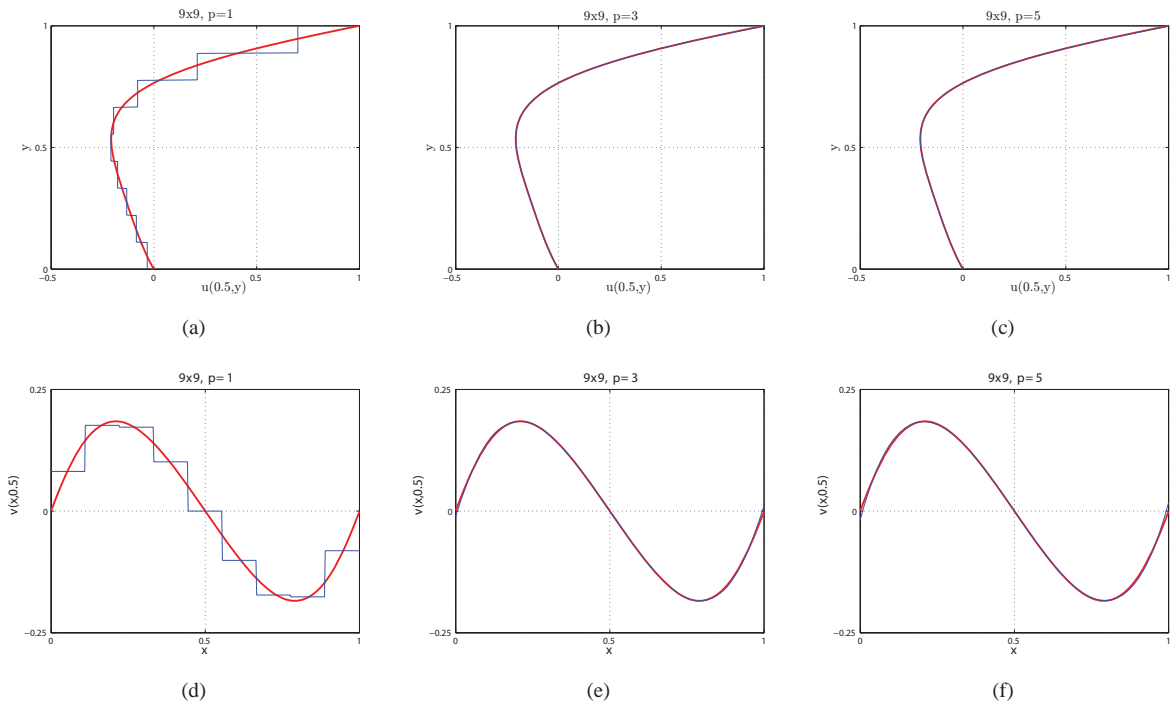


Figure 18: Comparison of numerical approximation (blue) with benchmark results of [40] (red). Horizontal (a,b,c) and vertical (d,e,f) velocity profile at centerlines of cavity for a 9x9 uniform grid of order 1, 3 and 5.

## 7. Conclusion

We have developed arbitrary order interpolants, from any basis that is a partition of unity, that satisfies a discrete Stokes theorem. The resulting gradient, curl and divergence conforming spaces have the property that the conservation laws become completely independent of the basis functions. As an example, we have derived conforming spaces from NURBS, and thereby generalized the discrete spaces of differential forms introduced in [1]. We have applied these new spaces in a mixed Galerkin setting which amongst others resulted in an exactly divergence free discretization of Stokes flow.

## References

- [1] A. Buffa, J. Rivas, G. Sangalli, R. Vázquez, Isogeometric Discrete Differential Forms in Three Dimensions, *SIAM Journal on Numerical Analysis* 49 (2011) 818.
- [2] W. Burke, *Applied differential geometry*, Cambridge Univ Pr, 1985.
- [3] J. Perot, Discrete conservation properties of unstructured mesh schemes, *Annual Review of Fluid Mechanics* 43 (2011) 299–318.
- [4] E. Tonti, On the formal structure of physical theories, *Istituto de matematica, Politecnico*, 1975.
- [5] E. Tonti, The reason for analogies between physical theories, *Applied Mathematical Modelling* 1 (1) (1976) 37–50.
- [6] C. Mattiussi, An analysis of finite volume, finite element, and finite difference methods using some concepts from algebraic topology, *Journal of Computational Physics* 133 (2) (1997) 289–309.
- [7] A. Bossavit, On the geometry of electromagnetism, *Journal of Japanese Society of Applied Electromagnetics and Mechanics* 6 (1998) 17–28 (no 1), 114–123 (no 2), 233–240 (no 3), 318–326 (no 4).
- [8] A. Bossavit, Computational electromagnetism and geometry, *Journal of the Japan Society of Applied Electromagnetics* 7,8 (2) (2000) 150–159 (no 1), 294–301 (no 2), 401–408 (no 3), 102–109 (no 4), 203–209 (no 5), 372–377 (no 6).
- [9] M. Desbrun, A. Hirani, M. Leok, J. Marsden, Discrete exterior calculus, *Arxiv preprint math/0508341*.
- [10] A. Hirani, *Discrete exterior calculus*, Ph.D. thesis, California Institute of Technology, 2003.
- [11] D. Arnold, R. Falk, R. Winther, Finite element exterior calculus, homological techniques, and applications, *Acta numerica* 15 (2006) 1–156.
- [12] D. Arnold, R. Falk, R. Winther, Finite element exterior calculus: from Hodge theory to numerical stability, *Bull. Amer. Math. Soc.(NS)* 47 (2) (2010) 281–354.
- [13] A. Buffa, G. Sangalli, R. Vázquez, Isogeometric analysis in electromagnetics: B-splines approximation, *Computer Methods in Applied Mechanics and Engineering* 199 (17-20) (2010) 1143–1152.

- [14] J. Evans, T. Hughes, Isogeometric Divergence-conforming B-splines for the Steady Navier-Stokes Equations, Tech. Rep., DTIC Document, 2012.
- [15] A. Back, E. Sonnendrücker, Spline discrete differential forms, in: ESAIM: PROCEEDINGS, vol. 35, 197–202, 2012.
- [16] A. Ratnani, E. Sonnendrücker, An Arbitrary High-Order Spline Finite Element Solver for the Time Domain Maxwell Equations, *Journal of Scientific Computing* (2012) 1–20.
- [17] P. Bochev, M. Gunzburger, A locally conservative mimetic least-squares finite element method for the Stokes equations, *Large-Scale Scientific Computing* (2010) 637–644.
- [18] P. Bochev, J. Hyman, Principles of mimetic discretizations of differential operators, *Compatible spatial discretizations* (2006) 89–119.
- [19] M. Bouman, A. Palha, J. Kreeft, M. Gerritsma, A conservative spectral element method for curvilinear domains, *Spectral and High Order Methods for Partial Differential Equations* (2011) 111–119.
- [20] M. Gerritsma, Edge functions for spectral element methods, *Spectral and High Order Methods for Partial Differential Equations* (2011) 199–207.
- [21] J. Kreeft, M. Gerritsma, Mixed Mimetic Spectral Element Method for Stokes Flow: A Pointwise Divergence-Free Solution, Arxiv preprint arXiv:1201.4409v2 .
- [22] J. Kreeft, M. Gerritsma, A priori error estimates for compatible spectral discretization of the Stokes problem for all admissible boundary conditions, Arxiv preprint arXiv:1206.2812 .
- [23] J. Kreeft, A. Palha, M. Gerritsma, Mimetic framework on curvilinear quadrilaterals of arbitrary order, Arxiv preprint arXiv:1111.4304 .
- [24] A. Palha, M. Gerritsma, Spectral element approximation of the Hodge-\* operator in curved elements, *Lecture Notes in Computational Science and Engineering* 76 LNCSE (2011) 283–291.
- [25] T. Hughes, J. Cottrell, Y. Bazilevs, Isogeometric analysis: CAD, finite elements, NURBS, exact geometry and mesh refinement, *Computer methods in applied mechanics and engineering* 194 (39-41) (2005) 4135–4195.
- [26] S. Lipton, J. Evans, Y. Bazilevs, T. Elguedj, T. Hughes, Robustness of isogeometric structural discretizations under severe mesh distortion, *Computer Methods in Applied Mechanics and Engineering* 199 (5-8) (2010) 357–373.
- [27] J. Cottrell, T. Hughes, Y. Bazilevs, *Isogeometric analysis: toward integration of CAD and FEA*, John Wiley & Sons Inc, 2009.
- [28] H. Flanders, *Differential forms with applications to the physical sciences*, vol. 11, Elsevier Science & Technology, 1963.
- [29] T. Frankel, *The geometry of physics: an introduction*, Cambridge Univ Pr, 2011.
- [30] A. Hatcher, *Algebraic topology*, Cambridge UP, 2002.
- [31] I. Singer, J. Thorpe, *Lecture notes on elementary topology and geometry*, Springer, 1976.
- [32] J. Dieudonne, *A history of algebraic and differential topology, 1900 - 1960*, Birkhauser, 1989.
- [33] Y. Bazilevs, L. Da Veiga, J. Cottrell, T. Hughes, G. Sangalli, Isogeometric analysis: approximation, stability and error estimates for h-refined meshes, *Mathematical Models and Methods in Applied Sciences* 16 (7) (2006) 1031.
- [34] J. Bramble, S. Hilbert, Estimation of linear functionals on Sobolev spaces with application to Fourier transforms and spline interpolation, *SIAM Journal on Numerical Analysis* 7 (1) (1970) 112–124.
- [35] C. Boor, A practical guide to splines, *Applied Mathematical Sciences* 27.
- [36] I. Schoenberg, Contributions to the problem of approximation of equidistant data by analytic functions: part AQ *Appl. Math* 4 (1946) 45–99.
- [37] L. Piegl, W. Tiller, *The NURBS book*, Springer Verlag, 1997.
- [38] F. Dubois, Vorticity–velocity–pressure formulation for the Stokes problem, *Mathematical methods in the applied sciences* 25 (13) (2002) 1091–1119.
- [39] V. Girault, P. Raviart, *Finite element methods for Navier-Stokes equations: theory and algorithms*, NASA STI/Recon Technical Report A 87 (1986) 52227.
- [40] M. Sahin, R. Owens, A novel fully implicit finite volume method applied to the lid-driven cavity problem, Part I: High Reynolds number flow calculations, *International journal for numerical methods in fluids* 42 (1) (2003) 57–77.